

#2

DOCUMENT ROOM 36-412  
RESEARCH LABORATORY OF ELECTRONICS  
MASSACHUSETTS INSTITUTE OF TECHNOLOGY  
CAMBRIDGE, MASSACHUSETTS 02139, U.S.A.

R.  
L.  
E.  
  
T  
E  
C  
H  
N  
I  
C  
A  
L  
  
R  
E  
P  
O  
R  
T  
  
4  
5  
7

# THE HAYSTACK-MILLSTONE INTERFEROMETER SYSTEM

ALAN E. E. ROGERS

Loan Copy  
only

---

TECHNICAL REPORT 457

MARCH 15, 1967

MASSACHUSETTS INSTITUTE OF TECHNOLOGY  
RESEARCH LABORATORY OF ELECTRONICS  
CAMBRIDGE, MASSACHUSETTS

The Research Laboratory of Electronics is an interdepartmental laboratory in which faculty members and graduate students from numerous academic departments conduct research.

The research reported in this document was made possible in part by support extended the Massachusetts Institute of Technology, Research Laboratory of Electronics, by the JOINT SERVICES ELECTRONICS PROGRAMS (U.S. Army, U.S. Navy, and U.S. Air Force) under Contract No. DA 36-039-AMC-03200(E); additional support was received from the National Aeronautics and Space Administration (Grant NsG-419).

Reproduction in whole or in part is permitted for any purpose of the United States Government.

Qualified requesters may obtain copies of this report from DDC.

MASSACHUSETTS INSTITUTE OF TECHNOLOGY

RESEARCH LABORATORY OF ELECTRONICS

Technical Report 457

March 15, 1967

THE HAYSTACK-MILLSTONE INTERFEROMETER SYSTEM

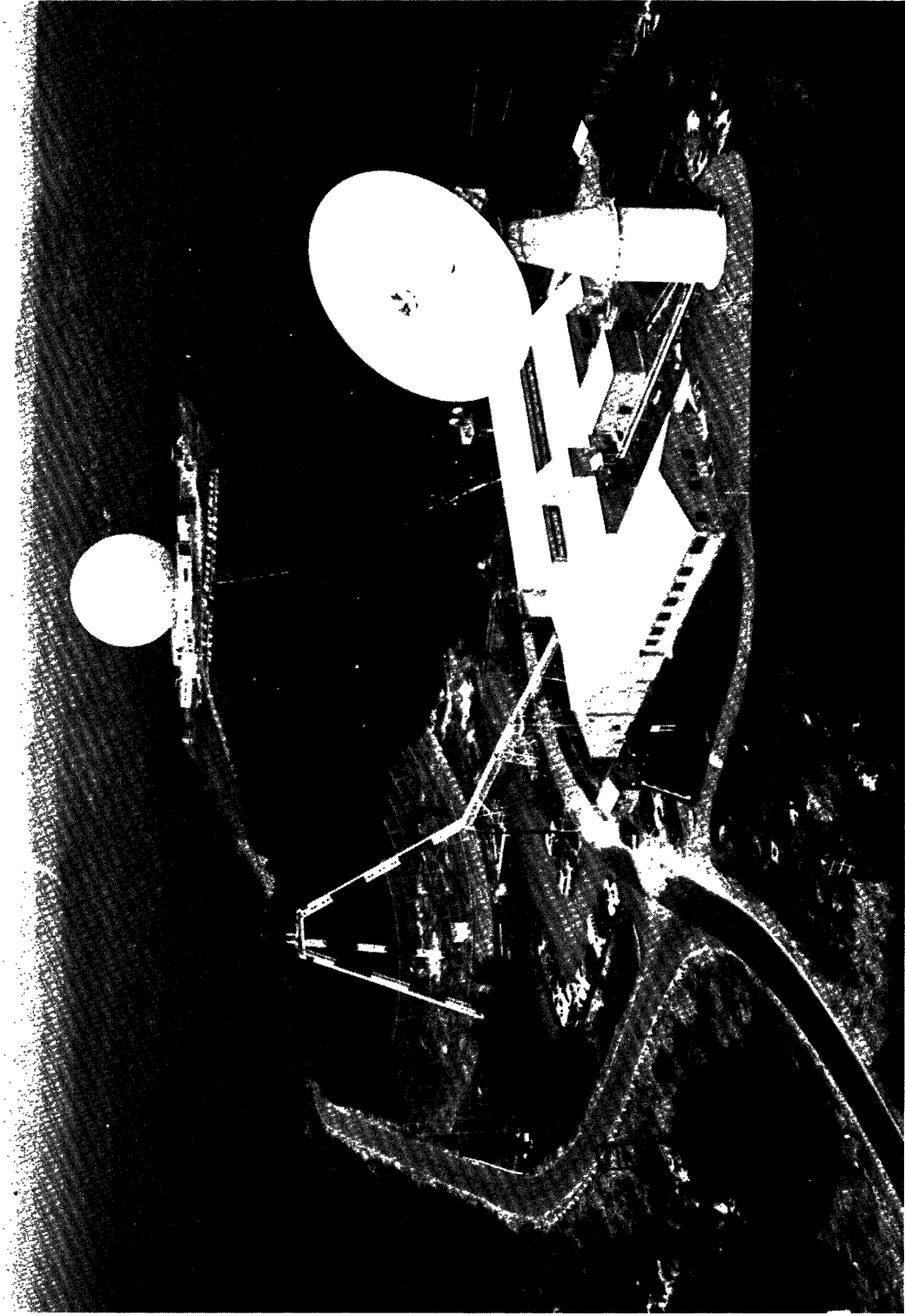
Alan E. E. Rogers

(Manuscript received January 13, 1967)

Abstract

The Haystack 120-ft antenna and the Millstone 84-ft antenna have been coupled together to form a radiometric interferometer. At 18-cm wavelength, which was chosen for a study of galactic OH emission, the interferometer has a minimum fringe spacing of 54 seconds of arc. The interferometer synthesizes a beam approximately equivalent to that of a 2000-ft parabolic antenna and can measure positions to a small fraction of the fringe spacing. The interferometer uses a digital correlator to analyze the fringe amplitude and phase as a function of frequency. This enables mapping of spectral features. The design and construction are described, as well as the theory and method of data reduction. A noise analysis shows that the threshold level could be reduced by using more complex processing techniques. It is shown that for radiometric studies many of the capabilities of a very large antenna can be synthesized, with smaller antennas and complex data-processing equipment taking the place of mechanical structure.





Haystack-Millstone Aerial View.



## TABLE OF CONTENTS

I.	INTRODUCTION	1
II.	DESIGN AND CONSTRUCTION	2
	2.1 Radio-Frequency Part of the System	2
	2.2 Intersite Coupling	2
	2.3 Digital Correlation and Data-Recording System	5
	2.4 Construction	5
	2.5 System Tests	5
III.	THEORY OF OPERATION AND METHOD OF DATA REDUCTION	9
	3.1 Geometry	9
	3.2 Computation of Spectral Fringe Amplitude and Phase	10
	3.3 Fringe Amplitude and Phase for Continuum Sources	13
	3.4 Normalized Autocorrelation Functions and Power Spectra from the Digital Correlator	14
	3.5 System Calibration	15
	3.6 Distribution of Brightness Temperature and Source Positions from Fringe Amplitude and Phase	17
	3.7 Computer Programs	19
IV.	INTERFEROMETER NOISE ANALYSIS	22
V.	POLARIZATION ANALYSIS	29
VI.	CONCLUSION	31
	APPENDIX Fortran Statement of the Program	32
	Acknowledgment	40
	References	41





## I. INTRODUCTION

The 120-ft antenna of the Haystack Microwave Research Facility and the 84-ft antenna of the Millstone Radar Facility used as an interferometer makes a powerful instrument for high resolution radiometric studies. The antennas are separated by approximately 2250 ft along a line approximately  $19^\circ$  East of North. This baseline gives a minimum fringe spacing of 54 seconds of arc at 18 cm and provides a good range of projected baseline for a wide range of declination. The convenient baseline, and the spectral processing equipment at Haystack make the system ideal for a study of OH emission regions that were unresolved with a single antenna.

This report describes the design and theory of the interferometer.

## II. DESIGN AND CONSTRUCTION

### 2.1 RADIO-FREQUENCY PART OF THE SYSTEM

A block diagram of the Millstone receiver front end is shown in Fig. 1. Circular and linear polarization is obtained from a dual-mode horn whose output ports give vertical and horizontal polarization. Combination of vertical and horizontal signals through a hybrid complex give left- and right-circular polarization after correct adjustment of the phase lengths. The antenna output is amplified by a tunnel diode amplifier and then filtered to reject the image band. A ferrite switch is included for calibration measurements. In the normal interferometer mode the switch remains switched to the antenna side. A noise source is used for single antenna measurements and system temperature measurement.

The local-oscillator signal is derived by phase-locking an oscillator to the sum or difference of a harmonic of 67 MHz and a signal whose frequency could be varied approximately 28 MHz. For the OH emission measurements the 24<sup>th</sup> harmonic was selected. The output of the oscillator was filtered to attenuate any spurious signals that tend to be produced by the synchronizer. A block diagram of the local-oscillator system is shown in Fig. 2.

The mixer output is amplified by a 30-MHz amplifier with a 10-MHz bandwidth. A line driver then boosts the level to 100 Mw. The Haystack receiver front end did not require the line driver, owing to its proximity to the control room where the IF outputs are combined. Otherwise the Haystack front end is similar to that at Millstone.

### 2.2 INTERSITE COUPLING

The intersite coupling of the radiometers involves the transmission of antenna-pointing commands to Millstone, remote control of the radiometer, transmission of the intermediate frequency to Haystack, and two-way coupling of the local-oscillator reference signals. To maintain good phase stability, the reference signals are transmitted along a servo-controlled line that nullifies line-length changes caused by temperature change and other effects. The transmission system also has to overcome a large line attenuation of 55 db for one-way transmission at 67 MHz. The selection of a lower basic frequency would have reduced attenuation but would have made phase-locking to L-band more difficult. A block diagram of the line servo is shown in Fig. 3. The 67-MHz reference signal is amplified to approximately 1 watt and transmitted to the line through a hybrid junction. At the receiving end of the line a portion of the signal is reflected. The reflected signal undergoes phase reversal with a 100-kHz rate as the diode switch modulates the reflection coefficient from  $+\frac{1}{2}$  to  $-\frac{1}{2}$ . Very little of the 100-kHz modulation is passed into the 67-MHz amplifier, because of the isolation afforded by the hybrid tee. At the transmitting end, the reflected signal is



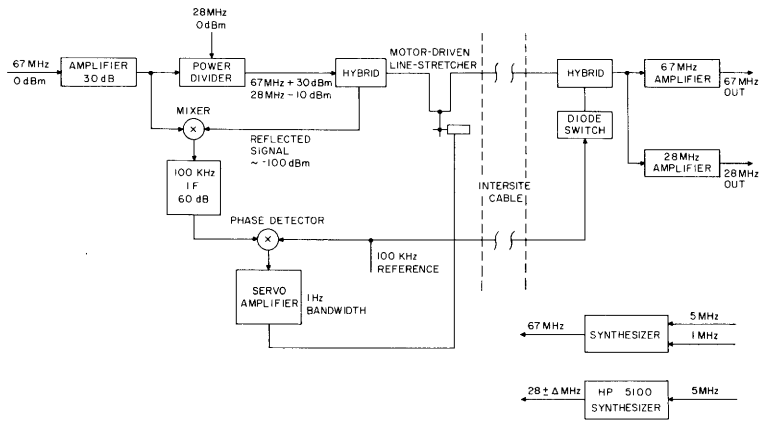


Fig. 3. Line servo to maintain phase stability.

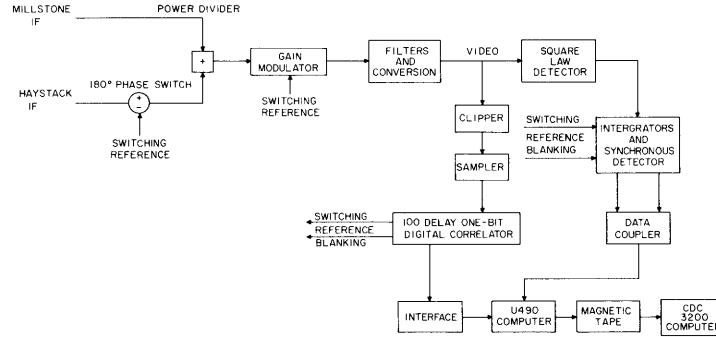


Fig. 4. Crosscorrelation scheme by addition and subtraction of IF signals.

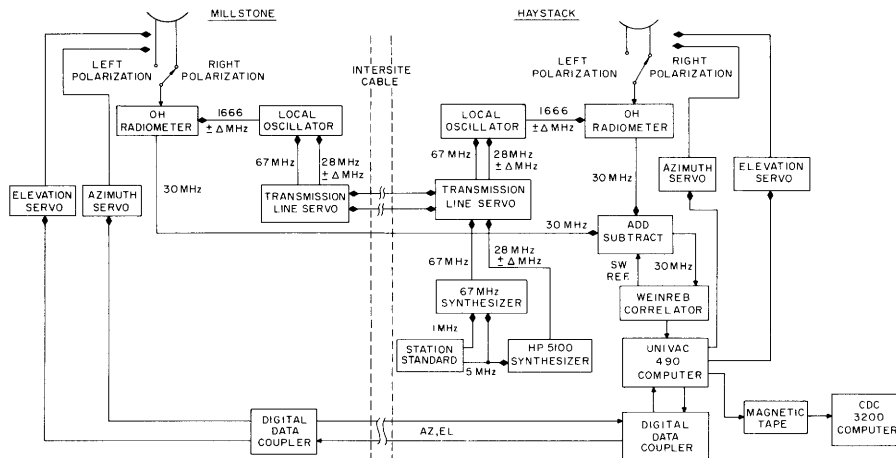


Fig. 5. Haystack-Millstone interferometer.

mixed with the 67-MHz reference signal and amplified. The output of the 100-kHz amplifier is proportional to  $\cos \phi \cos 2\pi ft$ , where  $f = 100$  kHz, and  $\phi$  is the phase of the 67-MHz signal after having traveled twice the line length. Multiplication of this signal by the 100-kHz reference signal produces the necessary error signal from the servo loop. The high loop gain makes it possible for the line servo to maintain a constant electrical line length to within a small fraction of an inch.

### 2.3 DIGITAL-CORRELATION AND DATA-RECORDING SYSTEM

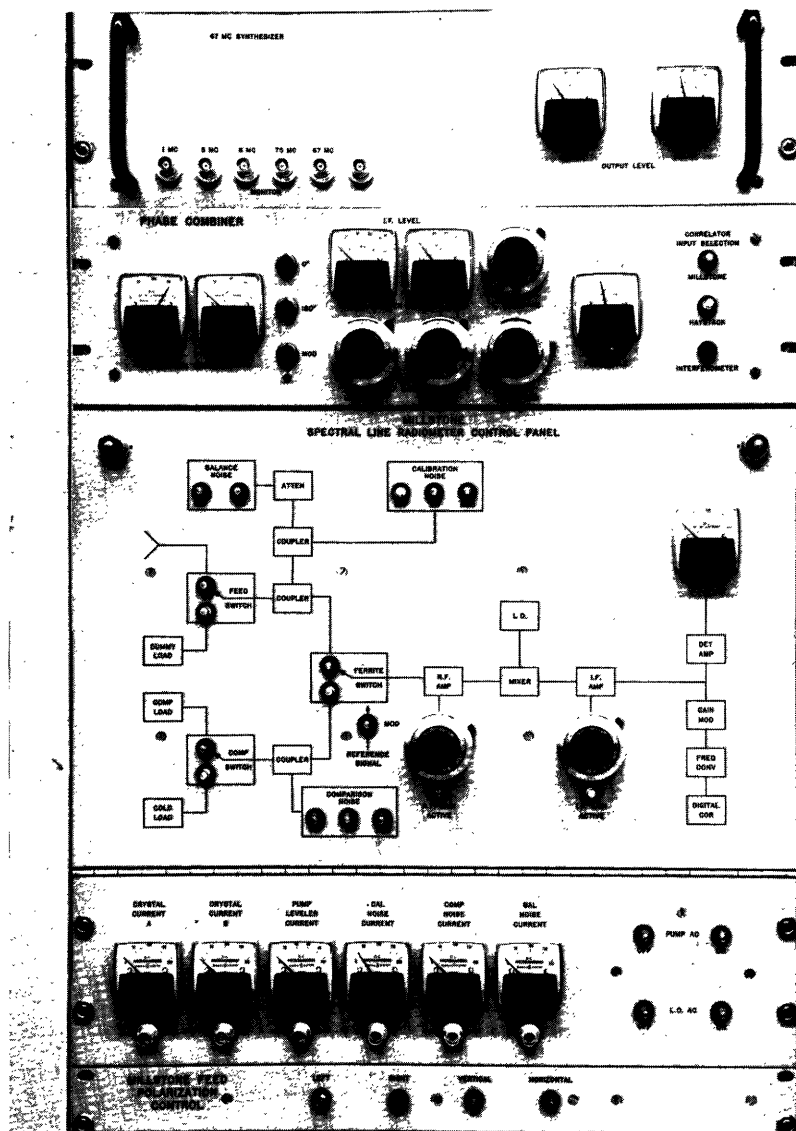
The IF signals are either added or subtracted as shown in Fig. 4. The combined signal is filtered and converted to video. The autocorrelation function of the clipped and sampled video signal is taken with a digital correlator. Autocorrelation functions of the sum and difference signals are transferred alternately to a computer every 100 msec. The basic correlation period is 87.5 msec. The system is blanked for 12.5 msec while the data are being transferred to the U490 computer. Signal bandwidths of 4 MHz, 1.2 MHz, 400 kHz, 120 kHz, and 40 kHz, can be analyzed by selecting appropriate filter and sampling frequencies. The autocorrelation function is a 16-bit binary word for each of 100 delays. An extra bit is used to indicate the state of the switching reference signal. The autocorrelation functions, together with continuum data, bandwidth and correlator mode, and antenna command azimuth and elevation are transferred to magnetic tape. A block diagram of the whole system is shown in Fig. 5.

### 2.4 CONSTRUCTION

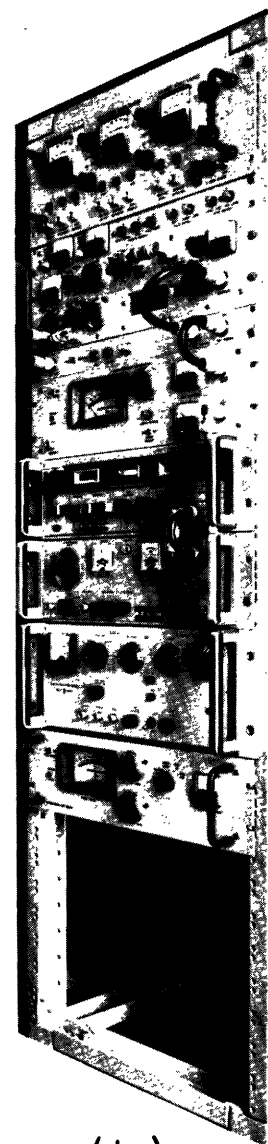
Figure 6 shows various sections of the interferometer equipment. The Millstone front end is located at the primary focus of the antenna, and the output of the tunnel diode amplifier is fed via a heliograph cable to the equipment box on the azimuth deck. The mixer and the local-oscillator system are located in the equipment box, which is connected by the intersite cables to the radiometer box at the Haystack secondary focus. The phase combiner and digital correlator are located in the Haystack control room from which both radiometers can be controlled by remote switching.

### 2.5 SYSTEM TESTS

Single-antenna measurements were made to measure the aperture efficiencies. The antenna temperatures of Cassiopeia A were 160°K and 180°K, which indicated efficiencies of 40% and 25% for the Millstone and Haystack antennas, respectively. The very low efficiency for Haystack is attributed to feed losses and the flow of energy past the Cassegranian subreflector which is in the near field of the feed horn at 18 cm. The efficiency of Millstone is close to what one would expect after

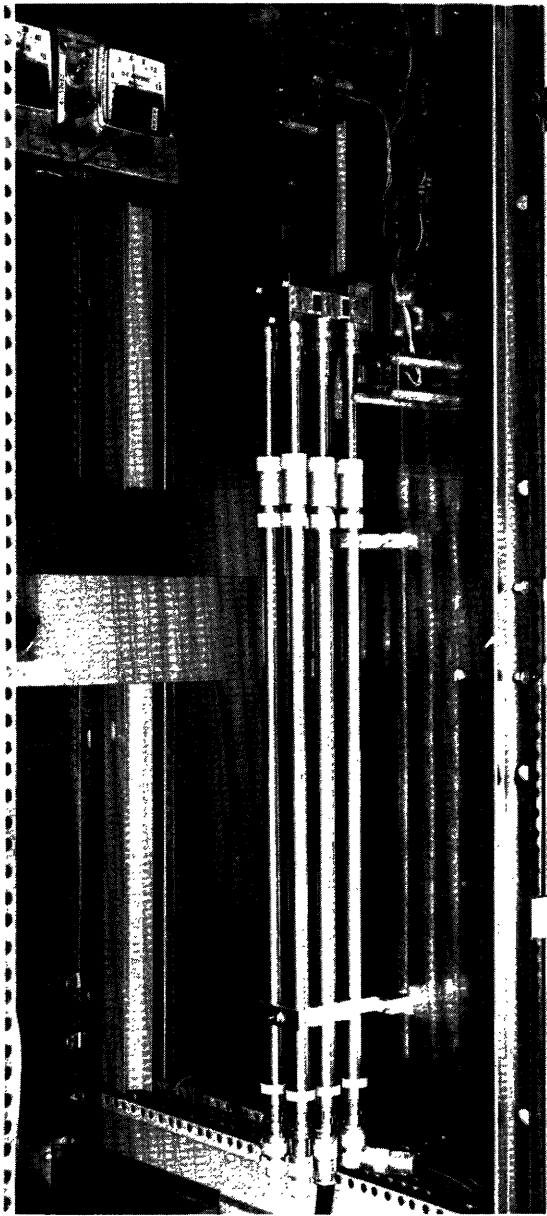


(a)

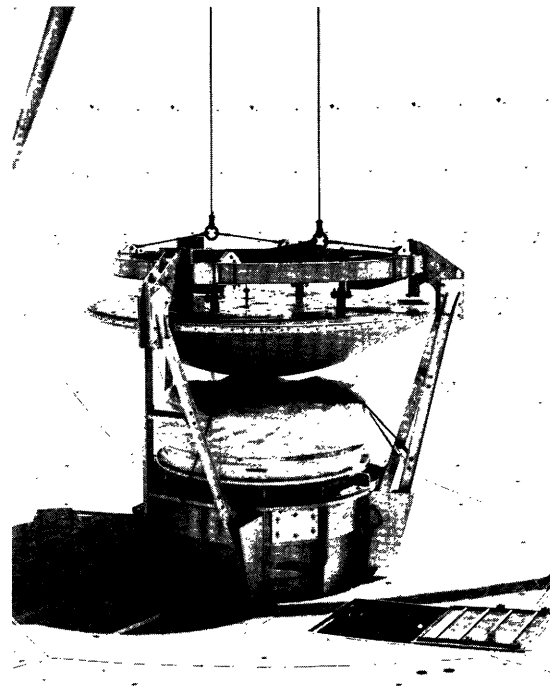


(b)

Fig. 6. (a) Control panel for the Millstone receiver.  
(b) Haystack receiver rack.



(c)



(d)

Fig. 6. (c) Motor-driven line stretcher.  
(d) Lowering of Millstone subreflector to make way for a prime-focus feed.

estimating the aperture blockage produced by the subreflector. For operation in the radiometric mode the Millstone subreflector was lowered to the vertex, as shown in Fig. 6d, to allow an L-band horn to be used at the primary focus.

After checking the individual radiometers for linearity, bandpass, and lack of spurious signals, the system was checked for phase coherence and phase stability. The test arrangement is illustrated in Fig. 7. A signal from a test oscillator is connected to each radiometer individually and then simultaneously. When the oscillator is swept in frequency the bandpass is displayed when only one radiometer is connected to the oscillator. When both radiometers are swept simultaneously fringes appear, because of the phase relationship between the radiometer outputs. The fringe spacing in Hz is the reciprocal of the delay in seconds. Measurement of the fringe pattern and bandpass functions showed that the phase noise in the system produced less than 2% reduction in fringe amplitudes. The phase stability was better than  $50^\circ$  during 24 hours. Some of this shift may have been due to the measuring technique, as observations of continuum radio sources indicated better stability.

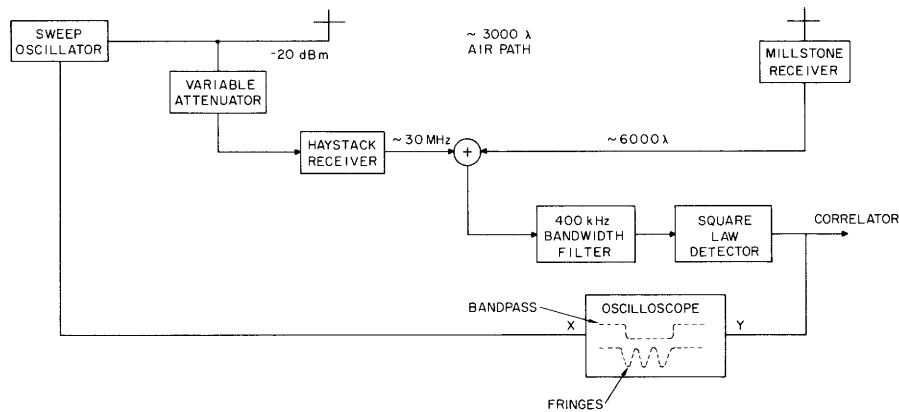


Fig. 7. Test arrangement for measuring phase coherence.

The trombone section of the line servo in Fig. 6c was observed to move approximately 5 ft during the sunrise and sunset period when the temperature changed about  $50^\circ\text{F}$ .

Finally, observations of unpolarized continuum radio sources with the interferometer confirmed the isolation between the two circular modes of the feeds to be better than 20 db.



### III. THEORY OF OPERATION AND METHOD OF DATA REDUCTION

#### 3.1 GEOMETRY

The interferometer geometry is shown in Fig. 8. Azimuth and elevation coordinates are centered at Haystack.  $\vec{r}_1$  is a fixed vector from the intersection of the azimuth axis and a horizontal plane through the elevation axis at Millstone to the intersection of the azimuth and elevation axes of Haystack.  $\vec{r}_2$  is the vector from the origin of  $\vec{r}_1$  to the intersection of a line to the source through the vertex intersecting the elevation axis of Millstone; therefore,  $\vec{r}_2$  is the offset of the elevation axis of Millstone from its azimuth axis.  $\hat{r}_3$  is a unit vector toward the apparent position of the source. If the source position is unknown, then  $\hat{r}_3$  is in the direction of a reference position in the sky relative to which the source distribution is to be mapped. These vectors may be expressed as

$$\vec{r}_1 = D \sin E_H \hat{i}_z + D \cos E_H \sin A_H \hat{i}_x + D \cos E_H \cos A_H \hat{i}_y \quad (1)$$

$$\vec{r}_2 = d \sin A_S \hat{i}_x + d \cos A_S \hat{i}_y \quad (\text{Differences in zenith neglected}) \quad (2)$$

$$\hat{r}_3 = \sin E_S \hat{i}_z + \cos E_S \sin A_S \hat{i}_x + \cos E_S \cos A_S \hat{i}_y, \quad (3)$$

where  $D$  is the distance between Haystack and Millstone,  $d$  is the offset of the elevation axis from the azimuth axis for the Millstone antenna,  $A_S$  and  $E_S$  are the apparent

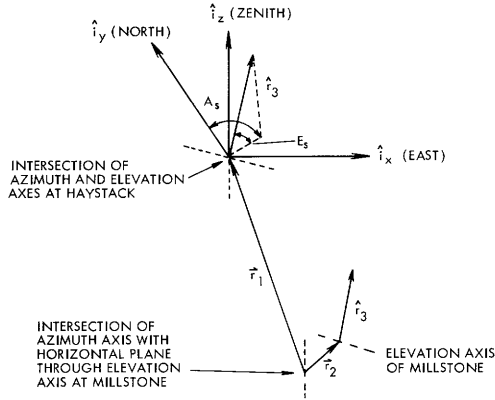


Fig. 8. Interferometer geometry.

azimuth and elevation of the source as seen from Haystack, and  $A_H$  and  $E_H$  are the azimuth and elevation of Haystack from Millstone in the Haystack coordinate system.

The portion of the interferometer delay which is azimuth- and elevation-dependent is given by

$$\begin{aligned} \tau_t &= \frac{1}{c} (\vec{r}_1 - \vec{r}_2) \cdot \hat{r}_3 \\ &= \frac{D}{c} \sin E_H \sin E_S + \frac{D}{c} \cos E_H \cos E_S \cos (A_S - A_H) - \frac{d}{c} \cos E_S. \end{aligned} \quad (4)$$

Since  $A_S$  and  $E_S$  is a function of time, so is  $\tau_t$ .

### 3.2 COMPUTATION OF SPECTRAL FRINGE AMPLITUDE AND PHASE

The signal from a point source is a plane wave that arrives at one antenna before the other. The spectrum of the delayed signal is the same, but the frequency components in the Fourier analysis of the signal are phase-shifted. If the signals are added, the power spectrum of the added signal is modulated. This can be seen in the following way: If we let  $x(t)$  be the received signal voltage,

$$x(\omega) = \int_{-\infty}^{+\infty} x(t) e^{-i\omega t} dt, \quad (5)$$

then the Fourier transform of the delayed signal is

$$x'(\omega) = \int_{-\infty}^{+\infty} x(t-\tau_i) e^{-i\omega t} dt = e^{-i\omega\tau_i} x(\omega). \quad (6)$$

The power spectra of the sum and difference of the signals with and without delay are

$$S_+(\omega) = |x(\omega)|^2 (2+2 \cos \omega\tau_i) \quad (7)$$

and

$$S_-(\omega) = |x(\omega)|^2 (2-2 \cos \omega\tau_i), \quad (8)$$

where  $S_+(\omega)$  and  $S_-(\omega)$  are the power spectra of the added and subtracted signals, respectively. The phase that results from the interferometer delay  $\tau_i$  can be expressed as the sum of component phases, according to the following equation.

$$\begin{aligned} \omega\tau_i &= (\omega_0 + \Delta\omega)(\tau_t + \tau_\ell + \tau') \\ &= \omega_0\tau_t + \omega_0\tau_\ell + \Delta\omega(\tau_t + \tau_\ell) + \omega\tau', \end{aligned} \quad (9)$$

where the delay is decomposed into  $\tau_t$  (as given in Eq. 4), the geometric delay for a reference position in the sky,  $\tau_\ell$ , the delay in the cables and amplifiers, and  $\tau'$ , the delay resulting from an offset of the point source from the reference point. The reference position is chosen to be the position toward which the main beams of the individual antennas are directed or the center of the region being mapped.  $\omega_0\tau_t$  is called the reference phase,  $\omega_0\tau_\ell$  the instrumental phase, and  $\Delta\omega(\tau_t + \tau_\ell)$  is a frequency-dependent phase.  $\omega\tau'$  is the phase developed, because of an offset of the point source from the reference phase. It is called the "fringe phase," since, in a complex source distribution, it is the phase of the Fourier component of the source distribution for the interferometer projected baseline at time  $t$ .  $\frac{\omega_0}{2\pi}$  is the center of the observed band, and  $\frac{\Delta\omega}{2\pi}$  is the frequency offset.  $\omega\tau_t$  produces a fringe pattern in the sky, and is a function of time owing to the earth's motion.

$\Delta\omega\tau_i$  produces fringes across the spectrum or equivalently expresses the dependence of the fringe pattern on frequency. When  $\Delta\omega\tau_i$  is small and there is only a fraction of a fringe over the analyzed spectrum, the interferometer is said to be in the "white fringe region." In a spectral interferometer it is only necessary to maintain the white-fringe condition over the resolution bandwidth, not the total bandwidth that is analyzed.

Thus far, only a point source has been considered. If it is assumed that different points in the sky radiate independently, then the receiver power spectrum will be just the summation of power spectra from the individual points and the difference power spectra becomes

$$S_D(\omega) = S_+(\omega) - S_-(\omega) = \sum_k |x_k(\omega)|^2 4 \cos \omega\tau_i. \quad (10)$$

The only portion of  $\omega\tau_i$  which changes with the summation variable,  $k$ , is  $\omega\tau'_k$ . Using complex quantities, we have

$$\begin{aligned} S_D(\omega) &= \sum_k |x_k(\omega)|^2 4 \operatorname{Re} e^{i\omega\tau_i} \\ &= 4 \operatorname{Re} e^{i(\omega_0\tau_t + \omega_0\tau_\ell + \Delta\omega(\tau_t + \tau_\ell))} \sum_k |x_k(\omega)|^2 e^{i\omega\tau'_k} \\ &= \operatorname{Re} A(\omega) e^{i\omega\tau'(\omega)} e^{i(\omega_0\tau_t + \omega_0\tau_\ell + \Delta\omega(\tau_t + \tau_\ell))}, \end{aligned} \quad (11)$$

where  $A(\omega)$  and  $\omega\tau'(\omega)$  are known as the fringe amplitude and phase. In summing over the elementary points that make up the source distribution, the resultant phase  $\omega\tau'(\omega)$  is a frequency-dependent quantity. The relation of these quantities to the brightness temperature distribution is discussed in section 3.6.

During one integration period, typically of 10 or 15 minutes, all of the phases except the reference phase  $\omega\tau_0$  remain constant to a few degrees for a source distribution contained within a few minutes of arc from the reference position. Limits for the rate of change of fringe and reference phases for the Haystack-Millstone baseline are given by

$$\frac{d\omega_0\tau_t}{dt} < 1 \text{ radian sec}^{-1}$$

$$\frac{d\omega_0\tau_\ell}{dt} \approx 0 \quad (\text{Phase-stable system})$$

$$\frac{d\Delta\omega(\tau_t + \tau_\ell)}{dt} < \frac{\Delta\omega}{\omega_0} \text{ radians sec}^{-1}$$

$$\frac{d\omega\tau'}{dt} < 3 \times 10^{-4} \text{ radians (minutes of arc displacement)}^{-1} \text{ sec}^{-1}.$$

The average fringe amplitude and phase over the integration period are determined by making a least-squares fit of the spectral difference to a function given in Eq. 11.

That is, we wish to minimize

$$\sum_t (S_{D,t}(\omega) - a(\omega) \cos \omega_0 \tau_t - b(\omega) \sin \omega_0 \tau_t)^2, \quad (12)$$

where

$$a(\omega) = A(\omega) \cos (\omega_0 \tau_\ell + \Delta\omega(\tau_0 + \tau_\ell) + \omega\tau'(\omega)) \quad (13)$$

$$b(\omega) = -A(\omega) \sin (\omega_0 \tau_\ell + \Delta\omega(\tau_0 + \tau_\ell) + \omega\tau'(\omega)) \quad (14)$$

$$\tau_0 = \frac{\tau_t + \tau_{(t+T)}}{2} \quad (15)$$

$$T = \text{Integration period.} \quad (16)$$

$S_{D,t}(\omega)$  is the power spectrum difference for a time interval from  $t - \frac{\Delta t}{2}$  to  $t + \frac{\Delta t}{2}$ . When the digital correlator is used,  $\Delta t = 200$  msec. The reference phase change  $\omega_0 \left( \tau_{t+\frac{\Delta t}{2}} - \tau_{t-\frac{\Delta t}{2}} \right)$  must be small for this fringe-filtering scheme to work satisfactorily; otherwise the fringes are smeared in the difference spectrum. The addition of a frequency offset in one of the local oscillators can obviate this problem, but this was unnecessary for the Haystack-Millstone interferometer.

Minimizing the expression above, we obtain

$$\omega\tau'(\omega) = \underbrace{\tan^{-1} \left( \frac{RX(\omega) - PY(\omega)}{QX(\omega) - RY(\omega)} \right)}_{\text{with quadrant identification}} - \Delta\omega(\tau_0 + \tau_\ell) - \omega_0 \tau_\ell \quad (17)$$

and

$$A(\omega) = \left\{ \frac{Y^2(\omega)(R^2 + P^2) + X^2(\omega)(Q^2 + R^2)}{(PQ - R^2)^2} \right\}^{1/2}, \quad (18)$$

where

$$X(\omega) = \sum_t S_{D,t}(\omega) \cos \omega_0 \tau_t \quad (19)$$

$$Y(\omega) = \sum_t S_{D,t}(\omega) \sin \omega_0 \tau_t \quad (20)$$

$$P = \sum_t \cos^2 \omega_o \tau_t \quad (21)$$

$$Q = \sum_t \sin^2 \omega_o \tau_t \quad (22)$$

$$R = \sum_t \sin \omega_o \tau_t \cos \omega_o \tau_t. \quad (23)$$

The sine-cosine multiplications can be performed on the autocorrelation functions before taking a Fourier transform by interchanging the order of summation. In practice, this is done to save computation time.

### 3.3 FRINGE AMPLITUDE AND PHASE FOR CONTINUUM SOURCES

For a continuum source  $\tau'$  is not a function of  $\omega$  and neither is the fringe amplitude  $A$  a function of  $\omega$ , provided the source spectrum is flat. Since determining spectral fringe phase and amplitude for a continuum source gives no additional information, and we would like to reduce the noise in the measurement by averaging over the bandwidth, it is desirable to modify the fringe filtering process. To do this, the least-squares fit is determined by summation over frequency in addition to time.

$$\sum_{\omega} \sum_t (S_{D,t}(\omega) - a \cos \omega_o \tau_t - b \sin \omega_o \tau_t)^2 = \text{minimum}. \quad (24)$$

Here we have used the following definitions:

$$a = A \cos (\omega_o \tau_{\ell} + \Delta\omega(\tau_o + \tau_{\ell}) + \omega\tau') \quad (25)$$

$$b = -A \sin (\omega_o \tau_{\ell} + \Delta\omega(\tau_o + \tau_{\ell}) + \omega\tau') \quad (26)$$

$$\omega\tau' = \tan^{-1} \left( \frac{Y_c + X_s}{Y_s - X_c} \right) - \omega_o \tau_{\ell} \quad (27)$$

$$A \approx \left\{ \frac{(X_s + Y_c)^2 + (Y_s - X_c)^2}{\left( \sum_{\omega} \sum_t \frac{1}{2} \right)^2} \right\}^{1/2}, \quad (28)$$

where

$$Y_c = \sum_{\omega} Y(\omega) \cos \Delta\omega(\tau_o + \tau_{\ell}) \quad (29)$$

$$Y_S = \sum_{\omega} Y(\omega) \sin \Delta\omega(\tau_0 + \tau_\ell) \quad (30)$$

$$X_C = \sum_{\omega} X(\omega) \cos \Delta\omega(\tau_0 + \tau_\ell) \quad (31)$$

$$X_S = \sum_{\omega} X(\omega) \sin \Delta\omega(\tau_0 + \tau_\ell). \quad (32)$$

The exact expressions for  $A$  and  $\omega\tau'$  involve a large number of terms that are very small when  $\Delta\omega(\tau_0 + \tau_\ell)$  undergoes a change of a few radians over the bandwidth that is analyzed. When a 1-bit correlator is used only the normalized power spectrum is obtained, so that it is impossible to obtain any fringe amplitude and phase information unless  $\Delta\omega(\tau_0 + \tau_\ell)$  is large enough to produce many fringes across the bandwidth.

Note that if the summation over  $\omega$  is done first, then in the case of a white-fringe compensated system ( $\Delta\omega(\tau_0 + \tau_\ell) \ll 1$ ), the method is equivalent to a least-squares fit to the time-function output of an integrator preceded by a square-law detector and filter with a bandwidth of  $\Delta\omega/2\pi$ .

### 3.4 NORMALIZED AUTOCORRELATION FUNCTIONS AND POWER SPECTRA FROM THE DIGITAL CORRELATOR

A Weinreb digital autocorrelator was used to obtain the fringe amplitude and phase information from the combined IF signals.<sup>1</sup>

The normalized autocorrelation function  $\rho(\tau)$  is obtained from the clipped-signal autocorrelation function  $\rho_C(\tau)$  on the assumption of a Gaussian bivariate probability distribution for the signal<sup>2</sup>

$$\rho(\tau) = \sin \frac{\pi}{2} \rho_C(\tau). \quad (33)$$

The difference of normalized autocorrelation functions for the added and subtracted IF signals is given within 1% for most signals in radio astronomy by

$$D_{k,t} = \frac{(A_{k,t} - B_{k,t+100 \text{ msec}})^\pi}{A_{1,t}} \quad k = 1, \dots, 100. \quad (34)$$

$A_{k,t}$  and  $B_{k,t}$  (regarding positive signal as logical 1 and negative signal as logical 0) are the counter output numbers for the added and subtracted signals, respectively. The subscript  $k$  designates the delay number (1, ... 100 for the Haystack correlator).  $k = 1$  corresponds to zero delay and consequently is just the number of samples in the integration period. This approximation to the clipping correction was made to save computer time.

The normalized difference power spectrum is obtained by taking the Fourier transform

$$S_{D,t}(i) = 2 \sum_{k=2}^{100} w_k D_{k,t} \cos \left[ \frac{2\pi(i-1)(k-1)}{400} \right] \quad i = 1, \dots, 200 \quad (35)$$

$$w_k = \frac{1}{2} + \frac{1}{2} \cos \frac{\pi(k-1)}{100}, \quad (36)$$

where  $w_k$  is a cosine weighting function, and  $i$  is the frequency channel number. Usually only channels 21 to 181 are used, as these are limits where the bandpass function starts to drop. The frequency offset  $\frac{\Delta\omega}{2\pi}$  is given by

$$\Delta\omega = \frac{(i-101)2\pi BW}{160}, \quad (37)$$

where  $BW$  is the bandwidth between channels 21 to 181, a quantity available to the U490 computer via the data coupler. The filter section before the correlator is designed so that channel 101 corresponds to 30.0 MHz in the IF spectrum.

The power spectrum is converted to a temperature scale by multiplying by the system temperature and dividing by the normalized power spectrum of the noise entering the clipper. This is an approximation that only holds for signal power much less than receiver noise power. The power spectrum obtained without knowledge of the signal power integrated over the bandwidth has a zero as the average value of the spectrum. The effect of this on the interferometer data is to produce an apparent fringe phase in portions of the spectrum where there is no signal. In practice, the effect is small, but it can be taken out of the data with a knowledge of the spectrum from single-antenna measurements. The exact expression for the difference spectrum in °K is given below.

$$S_{BP}(i) S_{D,t}(i) = S_{n,t}(i)(T_S + R_{x,t}(0)) - S_{n,t'}(i)(T_S + R_{x,t'}(0)) \quad (38)$$

$$\approx T_S(S_{n,t}(i) - S_{n,t'}(i)) \quad (39)$$

$$\text{for } R_{x,t}(i), R_{x,t'}(i) \approx 0,$$

where  $S_{BP}(i)$  is the bandpass function of the radiometer,  $R_{x,t}(0)$  and  $R_{x,t'}(0)$  are the signal temperatures at time  $t$  and  $t'$ , respectively, averaged over the bandpass.  $S_{n,t}(i)$  and  $S_{n,t'}(i)$  are the Fourier transforms of  $\sin \frac{\pi}{2} \rho_{c,t}(\tau)$ , and  $\sin \frac{\pi}{2} \rho_{c,t'}(\tau)$ . The approximation made to this expression only holds for continuum sources when there are many fringes across the bandwidth as we have mentioned.

### 3.5 SYSTEM CALIBRATION

The normalized fringe amplitude of a point source or of one that is not resolved by the interferometer is defined to be one. If it is not possible to make measurements with

zero spacing, it is necessary to calibrate the interferometer. There are two methods of calibration, both of which may be useful, the choice depending on the circumstances. The first method is to use measurements made with each antenna and radiometer individually. The individual radiometers are calibrated and the system temperatures measured. If the proportion of power from each radiometer is  $\beta$ , then the radiometer signals added can be written

$$\sqrt{\beta} \frac{\sqrt{T_{A1}}}{\sqrt{T_{S1}}} S_1(t) + \sqrt{\beta} n_1(t) + \frac{\sqrt{T_{A2}}}{\sqrt{T_{S2}}} S_2(t) + n_2(t), \quad (40)$$

and the subtracted signals as

$$\sqrt{\beta} \frac{\sqrt{T_{A1}}}{\sqrt{T_{S1}}} S_1(t) + \sqrt{\beta} n_1(t) - \frac{\sqrt{T_{A2}}}{\sqrt{T_{S2}}} S_2(t) - n_2(t), \quad (41)$$

where  $S_1(t)$  and  $S_2(t)$  are the power-normalized signal time functions, and  $n_1(t)$  and  $n_2(t)$  are the power-normalized receiver noise time functions. Since  $n_1(t)$  and  $n_2(t)$  are uncorrelated,

$$T_S = \frac{(\beta+1)}{2} \sqrt{T_{S1} T_{S2}}, \quad (42)$$

where  $T_S$  is the over-all system temperature,  $T_{S1}$  is the system temperature of receiver 1,  $T_{S2}$  is the system temperature of receiver 2, and

$$\beta = \frac{\text{power level from receiver 1}}{\text{power level from receiver 2}}.$$

With the system temperature defined in this manner, the fringe amplitude in  $^{\circ}\text{K}$  corresponding to a normalized fringe amplitude of one (a point source) is

$$2\sqrt{\beta} \sqrt{T_{A1} T_{A2}}, \quad (43)$$

where  $T_{A1}$  and  $T_{A2}$  are the individual antenna temperatures. Fringe amplitudes can be normalized by dividing this expression. In order to optimize the signal-to-system temperature ratio

$$\frac{4\sqrt{\beta} \sqrt{T_{A1} T_{A2}}}{\beta + 1} \frac{1}{\sqrt{T_{S1} T_{S2}}}, \quad (44)$$

the ratio  $\beta$  is chosen so that  $\beta = 1$ , or the power levels are weighted equally. When this is done the signal-to-system temperature ratio becomes

$$\frac{2\sqrt{T_{A1} T_{A2}}}{\sqrt{T_{S1} T_{S2}}}. \quad (45)$$



The second calibration method involves no system parameters and no calibration noise sources. The procedure is to measure the power spectrum of the source from each antenna while keeping the other just off the source. Loading switching is used to make the measurement. [The phase switching may be stopped and the signals just added, since the phase switching clearly has no effect in this mode.] If the signal were originating from a point source, then the fringe amplitude would be

$$\begin{aligned} A(\omega) &= \left\{ \left( \sqrt{S_1(\omega)} + \sqrt{S_2(\omega)} \right)^2 - \left( \sqrt{S_1(\omega)} - \sqrt{S_2(\omega)} \right)^2 \right\} \\ &= 4\sqrt{S_1(\omega)S_2(\omega)}, \end{aligned} \quad (46)$$

where  $S_1(\omega)$  and  $S_2(\omega)$  are the spectra from each antenna, with load switching used. Fringe amplitudes can thus be normalized by dividing by  $4\sqrt{S_1(\omega)S_2(\omega)}$ .

### 3.6 DISTRIBUTION OF BRIGHTNESS TEMPERATURE AND SOURCE POSITIONS FROM FRINGE AMPLITUDE AND PHASE

The fringe amplitude and phase provide information on the source distribution. For a general spatial distribution of incident flux, under the assumption of statistical independence of the plane waves that make up the expansion, the brightness temperature distribution and complex fringe amplitude are related by the following transform pair

$$A_{k, \ell}(\omega) e^{i\omega\tau'_{k, \ell}(\omega)} = \frac{2}{4\pi} \iint T_B(\omega, x, y) e^{ikx} e^{i\ell y} \sqrt{G_1(\omega, x, y)G_2(\omega, x, y)} dx dy \quad (47)$$

$$\iint A_{k, \ell}(\omega) e^{i\omega\tau'_{k, \ell}(\omega)} e^{-ikx} e^{-i\ell y} dk d\ell = \frac{2}{4\pi} 4\pi^2 \sqrt{G_1(\omega, x, y)G_2(\omega, x, y)} T_B(\omega, x, y), \quad (48)$$

where  $T_B(\omega, x, y)$  is the brightness temperature at a point located at a distance  $x$  parallel to the direction of increasing Right Ascension and a distance  $y$  in Declination from the reference point.  $G_1(\omega, x, y)$ ,  $G_2(\omega, x, y)$  are the antenna gains which may be taken outside the integral, in most instances, when the region mapped with the interferometer is much smaller than the beam patterns.  $k$  and  $\ell$  are the spatial fringe frequencies and are the coordinates of the transform or fringe-amplitude plane.

$$k = \frac{\partial \omega\tau_t}{\partial x}, \quad \ell = \frac{\partial \omega\tau_t}{\partial y}. \quad (49)$$

A plot of the coverage of the fringe-amplitude plane for the fixed-baseline Haystack/Millstone interferometer is shown for several sources in Fig. 9.

For a fixed baseline interferometer,

$$\omega\tau_t = \frac{\omega D}{c} \{ \sin \delta_B \sin \delta_S + \cos \delta_B \cos \delta_S \cos (L_S - L_B) \}, \quad (50)$$

so that

$$k = N \cos \delta_B \sin (L_S - L_B) \quad (51)$$

$$l = N \sin \delta_B \cos \delta_S - N \cos \delta_B \sin \delta_S \cos (L_S - L_B) \quad (52)$$

where

$L_S$  = Hour Angle of the source

$L_B$  = Hour Angle of the baseline

$\delta_S$  = Declination of the source

$\delta_B$  = Declination of the baseline

$N$  = Number of wavelengths in the baseline.

The brightness temperature can be obtained by taking the Fourier transform of the fringe amplitude and phase function. Unfortunately, a fixed-baseline interferometer

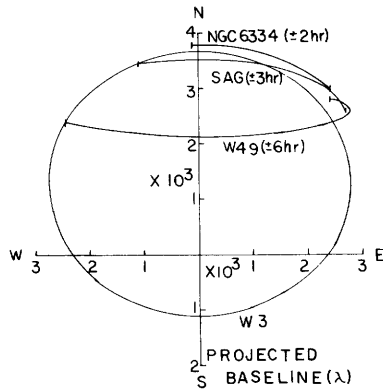


Fig. 9. Fringe-amplitude phase coverage for some OH sources. The limits shown are the observable limits.

has a very limited fringe-amplitude plane coverage, so that the transform analysis is not always used. Instead, the fringe amplitude and phase of certain model distributions are noted and compared with the observed fringe amplitude and phase. For example, the normalized fringe amplitude of a uniform disc of radius  $R$  is

$$\left| \frac{J_1\left(\frac{R}{S} 2\pi\right)}{R\pi/S} \right|,$$

where  $J_1$  is the first-order Bessel function, and  $S$  is the fringe spacing.

$$\frac{1}{S^2} = k^2 + l^2. \quad (53)$$

The fringe phase for a disc is

$$\omega\tau' = \frac{D\omega}{c} [(\sin \delta_B \cos \delta_S) \Delta\delta_S + (\cos \delta_B \cos \delta_S \sin (L_S - L_B)) \Delta R. A. S - (\cos \delta_B \sin \delta_S \cos (L_S - L_B)) \Delta\delta_S] \quad (54)$$

where

$\Delta\delta_S$  = offset in Declination of center from the reference position

$\Delta R. A. S$  = offset in Right Ascension of center from the reference position

D = length of baseline.

The relations above are used to determine the position and effective source size limit when a source shows no amplitude variation with hour angle, other than that expected from the noise. The source position is determined by making a least-squares fit of the phases to an offset in position.

Other distributions that have simple fringe amplitude and phase functions are a double source which is given by vector addition of the vectors representing the complex amplitudes for the two point sources, and circularly symmetric sources which have zero phase.

### 3.7 COMPUTER PROGRAMS

Data processing for the Haystack-Millstone interferometer was done in two stages. First, a real-time data-processing program in the Univac-490 computer recorded auto-correlation functions on magnetic tape, together with timing and antenna pointing information, and provided a monitor on the operation of the system. The contents of this tape were then analyzed, at some later time, by a Fortran program on the CDC 3200 to derive fringe amplitude and phase.

#### a. Real-Time Program

For this experiment, the Haystack and Millstone antennas were controlled simultaneously by the Haystack Pointing System<sup>3</sup> in the Univac 490 computer. The system includes an on-line spectral-line data-processing program,<sup>4</sup> which was modified to allow the recording of autocorrelation functions from the digital autocorrelator at the rate of 1000 15-bit words per second. This option may be requested by the observer via the console typewriter, and does not interfere with the normal functioning of the program. Interleaved with these data records were partial system data records, which contain command pointing angles (in both celestial and horizon coordinates), computed refraction corrections, and time.

#### b. Fortran Fringe-Processing Program

The tape written in real time was processed by using a Fortran program. A

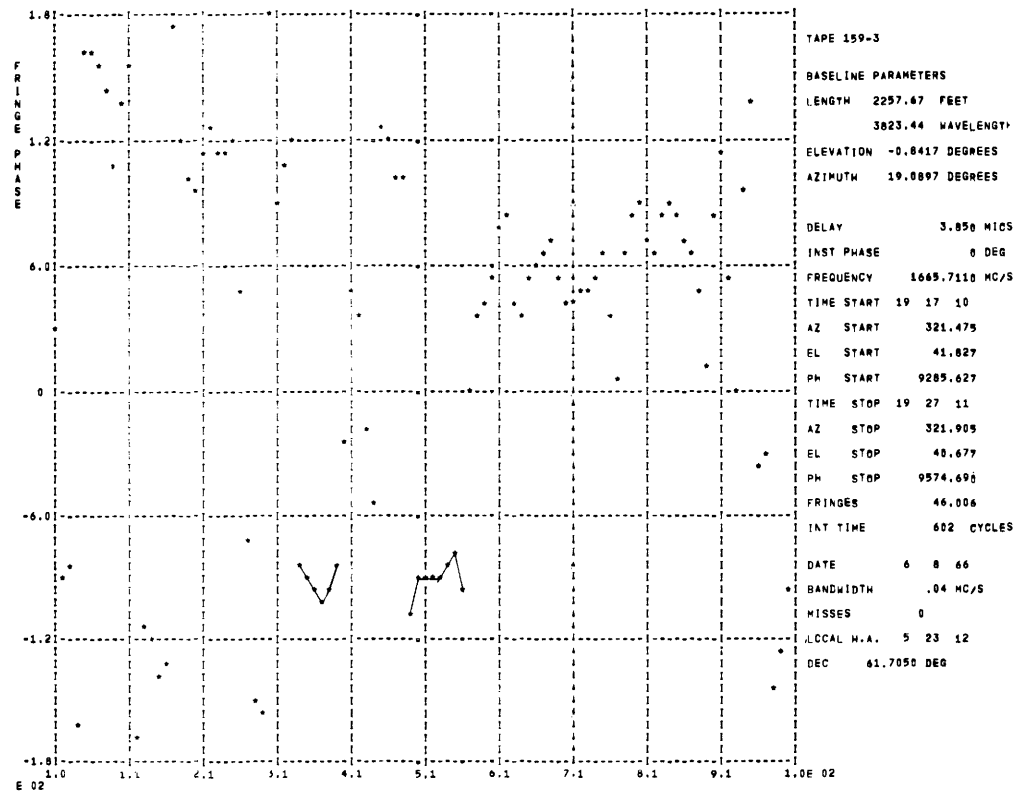
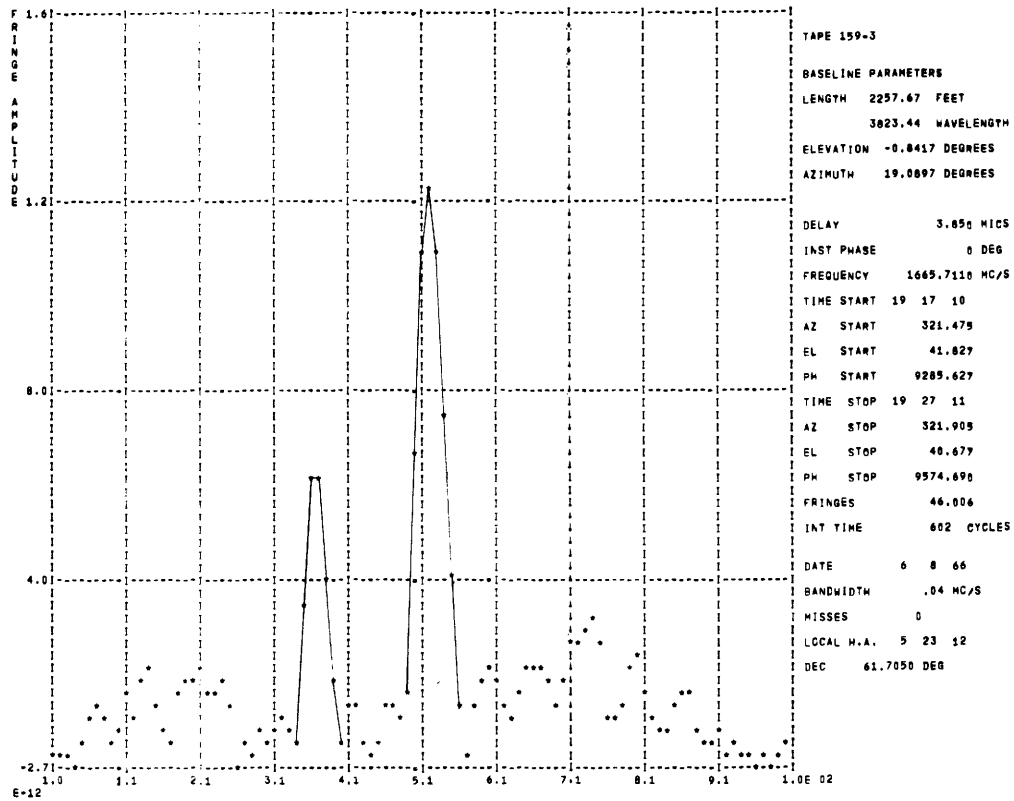


Fig. 10. High-speed printout of fringe amplitude and phase.

reference phase was computed by using the equation given in the section on interferometer geometry. The phase and amplitude were determined by the least-squares filtering technique discussed here. An example of the high-speed printout is shown in Fig. 10. The Fortran statement of the program is given in the appendix.

#### IV. INTERFEROMETER NOISE ANALYSIS

The difference spectrum  $S_{D,t}(\omega)$  for a sample of length  $\Delta t$  is made up of Gaussian noise from the two receivers plus signal noise. The receiver noise waveforms are assumed to be uncorrelated, while the signal noise is correlated.

$$S_{D,t}(\omega) = A(\omega) \cos \phi(\omega) \cos \omega_0 \tau_t - A(\omega) \sin \phi(\omega) \sin \omega_0 \tau_t + N_t(\omega), \quad (55)$$

where

$$\phi(\omega) = \omega_0 \tau_\ell + \Delta\omega(\tau_t + \tau_\ell) + \omega \tau'(\omega). \quad (56)$$

After digital filtering for a time  $T$ , during which  $\cos \omega_0 \tau_t$  goes through many cycles,

$$X(\omega) = PA(\omega) \cos \phi(\omega) + \sum_t N_t(\omega) \cos \omega_0 \tau_t \quad (57)$$

$$Y(\omega) = -QA(\omega) \sin \phi(\omega) + \sum_t N_t(\omega) \sin \omega_0 \tau_t \quad (58)$$

Quantities defined in Eqs. 19-22

since  $\sum_t \sin \omega_0 \tau_t \cos \omega_0 \tau_t \approx 0$ .

The signal and noise can be represented as the sum of two vectors

$$\vec{R} = \vec{A} + \vec{N}, \quad (59)$$

where

$$\vec{A} = A(\omega) \cos \phi(\omega) \hat{i}_x + A(\omega) \sin \phi(\omega) \hat{i}_y \quad (60)$$

$$\vec{N} = \frac{\sum_t N_t(\omega) \cos \omega_0 \tau_t}{P} \hat{i}_x - \frac{\sum_t N_t(\omega) \sin \omega_0 \tau_t}{Q} \hat{i}_y \quad (61)$$

where  $|\vec{R}|$  is the estimate of fringe amplitude.

The noise vector has uncorrelated components, since

$$\begin{aligned} & \overline{\sum_t N_t(\omega) \cos \omega_0 \tau_t \sum_t N_t(\omega) \sin \omega_0 \tau_t} \\ &= N_t^2(\omega) \sum_t \cos \omega_0 \tau_t \sin \omega_0 \tau_t = 0. \end{aligned} \quad (62)$$

Assume that  $\overline{N_t(\omega) N_{t+\Delta t}(\omega)} = 0$  and  $\sum_t \cos \omega_0 \tau_t \sin \omega_0 \tau_t = 0$ , which is a good approximation for long integration times.  $N_t(\omega)$  is a Gaussian random variable so that the components of  $N$  are independent Gaussian random variables with zero means and variances,  $\sigma^2$ . Joint probability distribution of the components is

$$p(a_x, a_y) = \frac{1}{2\pi\sigma^2} e^{-\frac{(a_x^2 + a_y^2)}{2\sigma^2}}, \quad (63)$$

where

$$a_x = |\vec{N}| \cos \theta \quad (64)$$

$$a_y = |\vec{N}| \sin \theta \quad (65)$$

so that (see Fig. 11)

$$P(|\vec{N}|) = \frac{|\vec{N}|}{\sigma^2} e^{-\frac{|\vec{N}|^2}{2\sigma^2}} \quad |\vec{N}| \geq 0 \quad (66)$$

$$p(\theta) = \frac{1}{2\pi} \quad 0 \leq \theta < 2\pi \quad (67)$$

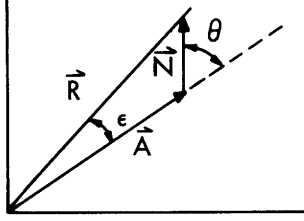


Fig. 11. Signal and noise vector.

The variance  $\sigma^2$  can be computed from the variance of  $N_t(\omega)$

$$\begin{aligned} \sigma^2 &= \frac{\overline{\sum_t N_t^2(\omega) \cos^2 \omega_0 \tau_t}}{\left(\overline{\sum_t \cos^2 \omega_0 \tau_t}\right)^2} \\ &= \frac{\frac{T}{\Delta t} \frac{1}{2} \overline{N_t(\omega)}}{\left(\frac{T}{\Delta t}\right) \frac{1}{4}} = \left(\frac{2\sqrt{2} a T_S}{\sqrt{T\Delta f}}\right)^2, \end{aligned} \quad (68)$$

where  $\Delta f$  is the frequency resolution of the spectral measurement, ( $a$ ) is a factor that normally is unity but equal to approximately 1.3 when the Weinreb correlator is used for spectral measurement. The additional factor of 2 arises from the fact that the difference spectrum is obtained by subtraction of two independent spectra, each made with integration time  $\Delta t/2$ .

The length of the noise vector has a Rayleigh distribution with mean

$$|\vec{N}| = \sqrt{\frac{\pi}{2}} \sigma = \sqrt{\frac{\pi}{2}} \frac{a T_S 2\sqrt{2}}{\sqrt{\Delta f T}} \quad (69)$$

as shown in Fig. 12.

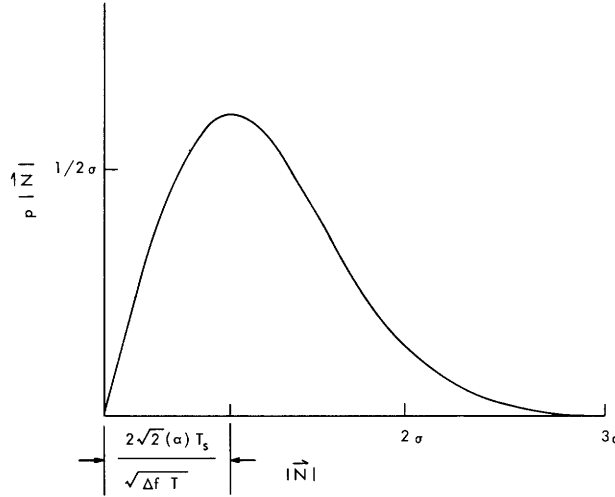


Fig. 12. Probability distribution of the amplitude of the noise vector.

The rms deviation of the amplitude and phase of the estimator is easily computed only for large signal-to-noise ratios when

$$\overline{|\vec{R}|^2} = \overline{|\vec{A}|^2} + \overline{|\vec{N}|^2} \quad (70)$$

$$\overline{|\vec{R}|} \approx \overline{|\vec{A}|} \quad (71)$$

and therefore

$$\Delta R_{\text{rms}} = \left( \overline{|\vec{N}|^2} \right)^{1/2} = \sqrt{2} \sigma = \frac{4aT_S}{\sqrt{\Delta f T}} \cdot K \quad (72)$$

$$\Delta \epsilon_{\text{rms}} = \left( \frac{\overline{|\vec{N}|^2} \overline{\sin^2 \theta}}{\overline{|\vec{A}|^2}} \right)^{1/2} = \frac{\sigma}{\overline{|\vec{A}|}} = \frac{2\sqrt{2} a T_S}{A \sqrt{\Delta f T}} \text{ radians,} \quad (73)$$

where A is in °K.

For any signal-to-noise ratio,

$$\Delta \epsilon_{\text{rms}} = \left\{ \int_0^{2\pi} \int_0^\infty \left( \tan^{-1} \left( \frac{|\vec{N}| \sin \theta}{|\vec{A}| + |\vec{N}| \cos \theta} \right) \right)^2 \frac{|\vec{N}|}{\sigma^2} e^{-\frac{|\vec{N}|^2}{2\sigma^2}} d\theta d|\vec{N}| \right\}^{1/2} \quad (74)$$

which reduces to the expression above for large signal-to-noise ratios.

In practice, signals weaker than  $\left( \overline{|\vec{N}|^2} \right)^{1/2}$  cannot be distinguished from the noise, and it is fairly reasonable to consider this to be the interferometer threshold. Figure 9, showing a plot of fringe spectral amplitude and phase, clearly illustrates the significance of the threshold.



The interferometer threshold can be reduced by using other schemes of processing. It will be shown that the system used here is a factor of 2 from optimum. The antenna signals for a point source can be considered for the purpose of this discussion. Signals from a more complex source are assumed to be the sum of uncorrelated components. The output of the two receivers can be written

$$x(t) = \sqrt{\tilde{T}_{A_1}} S(t) + \sqrt{T_{S_1}} n_1(t) \quad (75)$$

$$y(t) = \sqrt{\tilde{T}_{A_2}} S(t+\phi) + \sqrt{T_{S_2}} n_2(t), \quad (76)$$

where the function  $\phi$  is assumed to remain constant during the correlation time  $\Delta t$ . The spectrum of the receiver noise is assumed to be unity over the bandwidth considered. Spectral information is contained in the autocorrelation functions

$$\int_{-t'}^{t'} \langle x(t)x(t-\tau) \rangle e^{-i\omega\tau} d\tau = \tilde{T}_{A_1} S(\omega) + T_{S_1} + T_{S_1} S_{n_1}(\omega), \quad (77)$$

where  $S_{n_1}(\omega)$  is the noise in the measurement. The angular brackets denote time averaging over the integration period. Cross terms are omitted, under the assumption that the signal power is much less than the receiver noise.

$$\overline{S_{n_1}(\omega)} = 0 \quad (78)$$

$$\overline{S_{n_1}^2(\omega)} = \frac{1}{\Delta f \Delta t}, \quad (79)$$

where  $\Delta f$  is the spectral resolution, and  $\overline{S_{n_1}^2(\omega)}$  is the variance of spectral measurement derived under the assumption of Gaussian statistics for the noise. The information about  $\phi$  is contained in the crosscorrelation function,

$$\begin{aligned} 2 \int_{-t'}^{t'} \langle x(t)y(t-\tau) \rangle e^{-i\omega\tau} d\tau &= 2 \sqrt{\tilde{T}_{A_1} \tilde{T}_{A_2}} e^{-i\omega\phi} S(\omega) \\ &+ 2 \sqrt{T_{S_1} T_{S_2}} (\text{Re } S_n(\omega) + i \text{Im } S_n(\omega)), \end{aligned} \quad (80)$$

where the real and imaginary parts of the cross spectral function  $S_n(\omega)$  will be shown to be independent noise terms. The factor of 2 is introduced to make the signal equal to  $2 \sqrt{\tilde{T}_{A_1} \tilde{T}_{A_2}}$ .  $\tilde{T}_{A_1}$  and  $\tilde{T}_{A_2}$  are the average antenna temperatures over the bandwidth considered. That is,

$$\int_{-\infty}^{+\infty} T_A(\omega) \frac{d\omega}{2\pi} = \int_{-\infty}^{+\infty} \tilde{T}_A S(\omega) \frac{d\omega}{2\pi} = \tilde{T}_A. \quad (81)$$

The independence of  $\text{Re } S_n(\omega)$  and  $\text{Im } S_n(\omega)$  can be proved by showing them to be uncorrelated.

$$\begin{aligned}
\overline{\text{Re } S_n(\omega) \text{ Im } S_n(\omega)} &= \iint \overline{\langle n_1(t)n_2(t-\tau) \rangle} \overline{\langle n_1(t')n_2(t'-\tau') \rangle} \sin \omega\tau \cos \omega\tau' d\tau d\tau' \\
&= \iint \overline{\langle n_1(t)n_1(t') \rangle} \overline{\langle n_2(t-\tau)n_2(t'-\tau') \rangle} \sin \omega\tau \cos \omega\tau' d\tau d\tau' \\
&= 0.
\end{aligned} \tag{82}$$

To find the variance of  $\text{Re } S_n(\omega)$  and  $\text{Im } S_n(\omega)$ , consider the variance of the terms in the spectrum of added noise

$$\begin{aligned}
&\int_{-t'}^{t'} \langle (n_1(t)+n_2(t)) \langle (n_1(t-\tau)+n_2(t-\tau)) \rangle e^{-i\omega\tau} d\tau \\
&= S_{n_1}(\omega) + S_{n_2}(\omega) + \text{Re } S_n(\omega) + i \text{Im } S_n(\omega) + \text{Re } S_n(\omega) - i \text{Im } S_n(\omega).
\end{aligned} \tag{83}$$

The variance of the spectral estimate for the added signal is  $\frac{4}{\Delta f \Delta t}$  because adding the uncorrelated Gaussian signals gives a Gaussian signal with twice the power. Thus

$$\text{Var} \left[ S_{n_1}(\omega) + S_{n_2}(\omega) + 2 \text{Re } S_n(\omega) \right] = \frac{4}{\Delta f \Delta t}. \tag{84}$$

The individual terms are independent. Clearly,  $S_{n_1}(\omega)$  and  $S_{n_2}(\omega)$  are independent.  $S_{n_1}(\omega)$  and  $\text{Re } S_n(\omega)$  can be shown to be independent in the following manner.

$$\begin{aligned}
\overline{\text{Re } S_n(\omega) S_{n_1}(\omega)} &= \iint \overline{\langle n_1(t)n_1(t-\tau) \rangle} \overline{\langle n_1(t')n_2(t'-\tau') \rangle} \cos \omega\tau \cos \omega\tau' d\tau d\tau' \\
&= \iint \left( \overline{\langle n_1(t)n_1(t-\tau) \rangle} \overline{\langle n_1(t')n_2(t'-\tau') \rangle} \right. \\
&\quad + \overline{\langle n_1(t)n_1(t') \rangle} \overline{\langle n_1(t-\tau)n_2(t'-\tau') \rangle} \\
&\quad \left. + \overline{\langle n_1(t)n_2(t'-\tau') \rangle} \overline{\langle n_1(t-\tau)n_2(t') \rangle} \right) \cos \omega\tau \cos \omega\tau' d\tau d\tau' \\
&= 0,
\end{aligned} \tag{85}$$

since  $n_1$  and  $n_2$  are independent. Therefore

$$\text{Var} \left[ S_{n_1}(\omega) + S_{n_2}(\omega) + 2 \text{Re } S_n(\omega) \right] = \text{Var } S_{n_1}(\omega) + \text{Var } S_{n_2}(\omega) + \text{Var } 2 \text{Re } S_n(\omega), \tag{86}$$

so that

$$\text{Var } \text{Re } S_n(\omega) = \frac{1}{2\Delta f \Delta t}. \tag{87}$$

Table 1. Interferometer detection schemes and noise thresholds.

Interferometer Radiometer Type	Schematic	Noise Threshold $(\overline{N^2})^{1/2}$	Comments
1. Add-Subtract Autocorrelation	<p style="text-align: center;"><math>R_x + R_y \pm 2 \text{Re } R_{xy}</math></p>	$\frac{4 T_s}{\sqrt{\Delta f T}}$	$T_s = \sqrt{T_{s1} T_{s2}}$ If signal powers are added equally
2. Simultaneous Add-Subtract Autocorrelation	<p style="text-align: center;"><math>R_x + R_y + 2 \text{Re } R_{xy}</math> <math>R_x + R_y - 2 \text{Re } R_{xy}</math></p>	$\frac{2 \sqrt{2} T_s}{\sqrt{\Delta f T}}$	In schemes 1 and 2 for fringe reduction least squares fit is used and source motion required
3. Simultaneous Add-Subtract Autocorrelation with Quadrature	<p style="text-align: center;"><math>R_x + R_y + 2 \text{Re } R_{xy}</math> <math>R_x + R_y - 2 \text{Re } R_{xy}</math> <math>R_x + R_y + 2 \text{Im } R_{xy}</math> <math>R_x + R_y - 2 \text{Im } R_{xy}</math></p>	$\frac{2 T_s}{\sqrt{\Delta f T}}$	Optimum system if signals added in correct ratio to minimize $T_s$
4. Crosscorrelation	<p style="text-align: center;"><math>R_{xy}</math></p>	$\frac{2 T_s}{\sqrt{\Delta f T}}$	Optimum System . Fringe reduction does not require source motion $T_s = \sqrt{T_{s1} T_{s2}}$

The variance of  $\text{Im } S_n(\omega)$  is the same as the variance of  $\text{Re } S_n(\omega)$ . This can be shown by introducing  $90^\circ$  phase shift in  $x$  or  $y$ . Then

$$\begin{aligned} 2 \int_{-t'}^{t'} \langle x(t+a)y(t-\tau) \rangle e^{-i\omega\tau} d\tau &= 2 \int_{-t'}^{t'} \langle x(t)y(t-\tau') \rangle e^{i\omega a} e^{-i\omega\tau'} d\tau' \\ &= 2i e^{-i\omega\phi} \sqrt{\tilde{T}_{A_1} \tilde{T}_{A_2}} S(\omega) + 2\sqrt{\tilde{T}_{S_1} \tilde{T}_{S_2}} (-\text{Im } S_n(\omega) + i \text{Re } S_n(\omega)). \end{aligned} \quad (88)$$

If the crosscorrelation technique were applied to the signal from one antenna it would have an rms of  $\sqrt{2}$  times the rms for a total power radiometer. This is seen by setting  $\phi = 0$ , and considering only the real part of the transform. The signal is  $T_A$ , and the rms noise  $\frac{T_S \sqrt{2}}{\sqrt{\Delta f \Delta t}}$ . The factor of two is dropped for the signal, because of the 3 db lost in the division of power to the two receivers. When crosscorrelation is used to determine  $\phi$  and  $S(\omega)$ , the signal vector is  $2\sqrt{\tilde{T}_{A_1} \tilde{T}_{A_2}} S(\omega) e^{-i\omega\phi}$  and the noise vector, which has components  $2\sqrt{\tilde{T}_{S_1} \tilde{T}_{S_2}} \text{Re } S_n(\omega)$  and  $2\sqrt{\tilde{T}_{S_1} \tilde{T}_{S_2}} \text{Im } S_n(\omega)$ , each with variance  $\frac{2}{\Delta f \Delta t}$ , thus has an rms deviation of  $\frac{\sqrt{2} \sqrt{2} \sqrt{\tilde{T}_{S_1} \tilde{T}_{S_2}}}{\sqrt{\Delta f \Delta t}}$  (from Eq. 72). The averaging or filtering of the crosscorrelation functions to take out the time-variant component (resulting from the earth's rotation) of  $\phi$  is accomplished by multiplying by  $e^{\omega\tau_t}$  and summing. This is equivalent to the least-squares fit technique, but is much simpler, owing to the existence of the imaginary component.

The crosscorrelation function contains all the fringe information and the best estimate of this function must be the optimum system. It might be questioned whether it is the optimum scheme when it is clear that even if we know the fringe phase in advance of the source position and want to estimate the source flux, the system has  $\sqrt{2}$  more noise than a total power radiometer which is known to be optimum. If measurements of flux are to be made, however, with a total power radiometer, half the observing time should be spent determining the receiver noise power. The increase of  $\sqrt{2}$  in the noise of the crosscorrelation estimate is offset by the added information (receiver noise has been subtracted out) in the crosscorrelation function. Table 1 shows various interferometer detection schemes and their noise thresholds. One disadvantage of crosscorrelation should be noted. The spectral resolution obtainable with a crosscorrelator is half that of an autocorrelator with the same number of delays. The reason is that crosscorrelation functions are not symmetric, and require both positive and negative delays to extract the available information.

## V. POLARIZATION ANALYSIS

An interferometer can be used to analyze the polarization of a radio source. A complete set of polarizations can be obtained from the autocorrelation functions of two orthogonal polarizations plus the complex crosscorrelation function between the two polarizations. For right, left, and two sets of linear equations, we have

$$2S_R(\omega) = S_H(\omega) + S_V(\omega) + 2 \operatorname{Im} S_{H,V}(\omega) \quad (89)$$

$$2S_L(\omega) = S_H(\omega) + S_V(\omega) - 2 \operatorname{Im} S_{H,V}(\omega) \quad (90)$$

$$2S_{45^\circ}(\omega) = S_H(\omega) + S_V(\omega) + 2 \operatorname{Re} S_{H,V}(\omega) \quad (91)$$

$$2S_{-45^\circ}(\omega) = S_H(\omega) + S_V(\omega) - 2 \operatorname{Re} S_{H,V}(\omega) \quad (92)$$

where

$$S(\omega) = \int_{-\infty}^{+\infty} R(\tau) e^{-i\omega\tau} d\tau. \quad (93)$$

These relations are derived from the autocorrelation functions. For example,

$$\sqrt{2} x_R(t) = x_H(t) + x_V(t+90^\circ); \quad (94)$$

therefore,

$$2R_{x_R}(\tau) = R_{x_H}(\tau) + R_{x_V}(\tau) + R_{x_H x_V}(\tau-90^\circ) + R_{x_H x_V}(-\tau-90^\circ) \quad (95)$$

and hence

$$2S_R(\omega) = S_H(\omega) + S_V(\omega) + 2 \operatorname{Im} S_{H,V}(\omega). \quad (96)$$

When both elements of the interferometer have the same polarization, the autocorrelation function is measured. For example,

$$\int_{-\infty}^{+\infty} R_{x_V}(\tau-\phi) e^{-i\omega\tau} d\tau = e^{-i\omega\phi} S_V(\omega). \quad (97)$$

When the interferometer is used with elements having orthogonal polarizations the crosscorrelation function is obtained but real and imaginary parts of the Fourier transform can only be separated from the fringe phase information by making measurements with polarizations exchanged.

$$\int_{-\infty}^{+\infty} R_{x_H x_V}(\tau-\phi) e^{-i\omega\tau} d\tau = e^{-i\omega\phi} \{ \operatorname{Re} S_{H,V}(\omega) + i \operatorname{Im} S_{H,V}(\omega) \}, \quad (98)$$

while

$$\int_{-\infty}^{+\infty} R_{x_V x_H}(\tau-\phi) e^{-i\omega\tau} d\tau = e^{-i\omega\phi} \{ \operatorname{Re} S_{H,V}(\omega) - i \operatorname{Im} S_{H,V}(\omega) \}. \quad (99)$$

For an extended source, both of these measurements are required to obtain the polarization parameters over the source distribution. With the use of vertical and horizontal polarizations as an example, the Fourier transform of the fringe amplitude for vertical polarization yields the distribution of vertical polarization, and similarly for the horizontal polarization, while the distribution of right minus left and  $+45^\circ$  polarization minus  $-45^\circ$  polarization are given by the transform of the sum and difference of complex amplitudes made with one element of the interferometer vertical and the other horizontal, and vice versa.

## VI. CONCLUSION

This report shows that while a digital correlator (with phase switching), or a digital crosscorrelator, is useful for a spectral interferometer it also has many advantages when spectral information is not required. It is interesting to note that the optimum receiver system for making a radiometric map as a function of frequency and polarization, with two single-feed antennas used, consists of 4 receivers and 4 crosscorrelators: one receiver on each of the two orthogonal polarization ports of each antenna, and the crosscorrelators between pairs of receivers, one on each antenna.

APPENDIX

Fortran Statement of the Program

3200 FORTRAN (2.1)

```

PROGRAM MILSTAK
  DIMENSION CT(400),WK(100),F(241B),T(241B),ASUM(200),SC(310B),
1 PAR(23B),NH(102),ISUM(2,100,5),AZS(6),TIME(6),ELS(6),PH(6),
2   PWREF(5),X(100),Y(100),XT(200),YT(200),PHASE(200),
3 AMP(200),CPR(5),SPR(5),TITLE(21),PA(80),ANS(10),PHA(200),
4 LABELX(6),LABELY(8),KI(4),TIT(21),
5 INFO(364),PNH(102),U(100),Z(100),TRANS(200),NHT(28),CP(5),SP(5)
  COMMON ISUM,S,D,PHA,PHASE
  CHARACTER PA,PNH
  EQUIVALENCE (NH,PNH)
  INTEGER TITLE,REPLY,TIT,OT
  PIE=3.1415926536
  R=3.141592653/180.
  READ 1,DMIL,DBAS,ELB,AZB
1  FORMAT(4F10.4)
  CEB=COSF(ELB*R)
  SEB=SINF(ELB*R)
C  STORING TABLE FOR FOURIER TRANSFORM
  DO 78 I=1,400
78 CT(I)=COSF(2.*3.141592653*(I-1)/400.)
C  WK IS WEIGHTING FUNCTION FOR AUTOCORRELATION FUNCTIONS
  DO 17 K=1,100
17 WK(K)=.5+.5*COSF((3.14159*(K-1))/100.)
900 INUM=0
  WRITE(59,955)
955 FORMAT(37HNEW OUTPUT TAPE REQUIRES JUMP SW 2 ON)
  PAUSE
  ISRCH=3
  99 CONTINUE
  GO TO (928,929) SSWTCHF(2)
928 WRITE(59,930)
930 FORMAT(14HMOUNT NEW TAPE)
  PAUSE
  GO TO (961,929) SSWTCHF(2)
961 END FILE 20
  REWIND 20
929 CONTINUE
  INUM=INUM+1
  DO 77 I=1,5
77 TIME(I)=86400.
  DO 18 K=1,100
  Y(K)=0.
  U(K)=0.
18 X(K)=0.
  IREP=0
  IMIS=0
  IT=0.
  PP=0.
  QQ=0.
  RR=0.
  GO TO (3,3,119,184) ISRCH

```



```

184 ISRCH=2
    GO TO 119
C   READ INPUT PARAMETERS
119 WRITE(59,120)
120 FORMAT(28HTYPE T FOR CLIPPED TRANSFORM)
    READ(58,121) OT
121 FORMAT(A1)
    WRITE(59,101)
101 FORMAT(31H CENTER FREQUENCY IN MEGACYCLES)
    READ(58,102)PA
102 FORMAT(80R1)
    CALL NUMBERS(PA,80,ANS,NA)
    IF(NA)103,104,103
103 FREQ=ANS(NA)
104 WRITE(59,105)
105 FORMAT(47HINST PHASE IN DEGREES AND DELAY IN MICROSECONDS)
    READ(58,106)PA
106 FORMAT(80R1)
    CALL NUMBERS(PA,80,ANS,NA)
    IF(NA)108,109,108
108 PINST=ANS(NA-1)
    DELAY=ANS(NA)
109 WRITE(59,110) FREQ,PINST,DELAY
110 FORMAT(4HFREQ,F10.4,12HMC/S INST PH,F8.3,11H DEG  DELAY,F9.3,9H MI
1CROSEC)
    WRITE(59,112)
112 FORMAT(5HTITLE)
    READ (58,113) TIT
113 FORMAT(14A4)
    IF(TIT .EQ. 1H )123,124
124 DO 125 I=1,21
125 TITLE(I)=TIT(I)
123 WRITE(59,114)
114 FORMAT(6H HAPPY)
    READ(58,115) REPLY
115 FORMAT(A2)
    IF(REPLY.EQ. 2HNO) 119,116
116 CONTINUE
    WC=FREQ*12.*2.54000508/29979.29
    W=WC*DBAS
C
C *****
C
3 CALL INFREAD(F,T,ASUM,SC,PAR,NH,MODE,NINT,NBW,ISUM,NC)
C   NC   -1  PARITY ERROR
C       0  END OF FILE
C       2  TITLE
C       1  GEORGE'S PROGRAM
C       3  PARTIAL SYSTEMS RECORDING
C       5  CHANNEL 5
C       6  CHANNEL 6 (AUTOCORRELATION FUNCTIONS)
    NC=NC+2
    GO TO (100,300,200,400,500,600,700,800,600) NC
600 GO TO 3
400 CALL ICVT(2,19,KI,-1)
    KI(1)=KI(1)-1900
    DO 401 I=1,28
401 NHT(I)=NH(I)
    GO TO 3

```

```

100 WRITE(59,199)
199 FORMAT(23H PARITY ERROR, PRESS GO)
    PAUSE
    GO TO 3
500 GO TO (3,534,529) ISRCH
529 NHOUR=PAR(3)/3600.
    NMIN=(PAR(3)-NHOUR*3600.)/60.
    NSEC=PAR(3)-NHOUR*3600.-NMIN*60.
    WRITE(59,530) NHOUR,NMIN,NSEC
530 FORMAT(I4,6H HOURS,I4,4H MIN,I4,4H SEC)
    WRITE(59,531)
531 FORMAT(33H TYPE 1 SKIP, 2 PROCESS, 3 REINIT)
    READ (58,532) ISRCH
532 FORMAT(I1)
    GO TO (3,534,119) ISRCH
534 DO 501 L=1,5
    M=6-L
    AZS(M+1)=AZS(M)
    TIME(M+1)=TIME(M)
    ELS(M+1)=ELS(M)
C 501 PH(M+1)=PH(M)
    SOURCE COORD
    AZS(1)=PAR(1)
    ELS(1)=PAR(2)+PAR(4)
    TIME(1)=PAR(3)
    CES=COSF(ELS(1))
    SES=SINF(ELS(1))
C    COMPUTE REFERENCE PHASE PH(I)
    PH(1)=2.*3.141592653*WC*(DBAS*(SEB+SES+CEB+CES+COSF(AZS(1)-AZB+R))
1 -DMIL*CES/12.)
    PASC=PAR(5)
    DECL=PAR(6)
    GO TO 3
700 IF(MODE)3,701,3
701 BW=NBW
    BW=BW/1000.
    GO TO (702,3) SSWTCHF(5)
702 ISRCH=4
    GO TO 99

C
C *****
C
800 GO TO (3,880,3)ISRCH
880 IF(MODE)3,809,3
809 DO 802 I=2,6
    IF(PAR(1)-86384.)803,3,3
803 IF(PAR(1)-TIME(I))802,802,818
802 CONTINUE
    GO TO 3
818 DO 816 J=1,4
    IDIF=(PAR(J+1)-PAR(J))+40.*.5
    IF(IDIF=8) 817,816,817
817 IMIS=IMIS+1
816 CONTINUE
    DO 815 J=1,5
    IF(ISUM(1,1,J))811,3 ,811
C    COMPUTE REF PHASE AT TIME DATA IS TAKEN
811 PHREF(J)=PH(I)+(PH(I-1)-PH(I))*(PAR(J)-TIME(I))/(TIME(I-1)-TIME(I)
1)

```

```

      SPR(J)=SINF(PHREF(J))
      CPR(J)=COSF(PHREF(J))
      PP=PP+CPR(J)**2
      QQ=QQ+SPR(J)**2
      RR=RR+CPR(J)*SPR(J)
815 CONTINUE
      IT=IT+1
      IF(IT-1)806,807,806
807 P1=PHREF(1)
      T1=PAR(1)
      IH1=PAR(1)/3600.
      IM1=(PAR(1)-IH1*3600)/60.
      IS1=PAR(1)-IH1*3600=IM1*60
      XINT=(PAR(1)-TIME(I))/(TIME(I-1)-TIME(I))
      A1=(AZS(I)+(AZS(I-1)-AZS(I))*XINT)/R
      E1=(ELS(I)+(ELS(I-1)-ELS(I))*XINT)/R
C      SUM PRODUCTS OD AC FUNCS AND COSINE AND SINE OF PHASE
806 IF(OT.EQ.1HT)840,841
840 DO 842 J=1,5
      DO 842 K=1,100
842 U(K)=0.
841 DO 808 J=1,5
      CP(J)=CPR(J)*PIE/ISUM(1,1,J)
      SP(J)=SPR(J)*PIE/ISUM(1,1,J)
      DO 808 K=1,100
      DX=ISUM(1,K,J)-ISUM(2,K,J)
      X(K)=X(K)+DX*CP(J)
808 Y(K)=Y(K)+DX*SP(J)
      T2=PAR(5)
      A2=(A7S(I)+(AZS(I-1)-AZS(I))*(PAR(5)-TIME(I))/(TIME(I-1)-TIME(I)))
1/R
      E2=(ELS(I)+(ELS(I-1)-ELS(I))*(PAR(5)-TIME(5))/(TIME(I-1)-TIME(I)))
1/R
      GO TO 3
C
C      *****
C
300 WRITE(59,301)
301 FORMAT(11HEND OF TAPE)
      REWIND 30
      PAUSE
      GO TO 900
200 GO TO (279,204,279)ISRCH
279 ISRCH=3
      GO TO 3
204 P2=PHREF(5)
      IH2=T2/3600.
      IM2=(T2-IH2*3600.)/60.
      IS2=T2-IH2*3600=IM2*60
C      LOCAL HOUR ANGLE
      MH=PAR(5)/3600.
      PM=(PAR(5)-MH*3600.)/60.
      MS=PAR(5)-MH*3600.=MM*60.
      AZIM=(A2+A1)/2.
      ELEV=(E2+E1)/2.
      FR=(P2-P1)/(2.*3.1415926)
      DO 209 I=1,100
      U(I)=U(I)/(IT*5.)
      X(I)=X(I)/(IT*5.)
209 Y(I)=Y(I)/(IT*5.)

```

```

C   COMPUTE FOURIER TRANSFORM
DO 203 I=1,200
  XT(I)=0.
  YT(I)=0,
  TRANS(I)=0.
DO 203 K=2,100
  N=(I-1)*(K-1)-((I-1)*(K-1)/400)*400+1
  TRANS(I)= 2.*U(K)+WK(K)*CT(N)+TRANS(I)
  XT(I)=2.*X(K)+WK(K)*CT(N)+XT(I)
203  YT(I)=2.*Y(K)+WK(K)*CT(N)+YT(I)
DO 205 I=1,200
  XNUM=RR*XT(I)-PP*YT(I)
  XDEN=QQ*XT(I)-RR*YT(I)
  CALL ARCT(XNUM,XDEN,PHA(I))
  TAU=(P2+P1)/(2.*FREQ)+DELAY*2.*3.14159
C   SUBTRACT INSTRUMENTAL PHASE WHICH IS FREQ DEP
  PHASE(I)=PHA(I)-PINST*R-(I-101)*TAU*BW/160.
  IF(PHASE(I))220,222,221
221  NUMB=(PHASE(I)+3.141592653)/(2.*3.141592653)
  GO TO 223
220  NUMB=(PHASE(I)-3.141592653)/(2.*3.141592653)
223  PHASE(I)=PHASE(I)/R-NUMB*360.
222  IF(PHA(I))224,205,225
225  NUMB=(PHA(I)+3.141592653)/(2.*3.141592653)
  GO TO 227
224  NUMB=(PHA(I)-3.141592653)/(2.*3.141592653)
227  PHA(I)=PHA(I)/R-NUMB*360.
205  AMP(I)=SQRTF((YT(I)**2)*(RR**2+PP**2)*(XT(I)**2)*(QQ**2+RR**2)-
  1  2.*XT(I)*YT(I)*RR*(PP+QQ))*(I*5.)/(PP*QQ-R**2)
C   AVERAGE PHASE AND AMPLITUDE FOR CONTINUUM SOURCES
  YC=0.
  XC=0.
  YS=0.
  XS=0.
DO 207 I=21,181
  YC=YC+YT(I)*COSF((I-101)*TAU*BW/160,)
  YS=YS+YT(I)*SINF((I-101)*TAU*BW/160,)
  XC=XC+XT(I)*COSF((I-101)*TAU*BW/160,)
207  XS=XS+XT(I)*SINF((I-101)*TAU*BW/160,)
  XNUM=-YC-XS
  XDEN=XC-YS
  CALL ARCT(XNUM,XDEN,PCAL)
  PCAL=PCAL/R-PINST
  PAMP=SQRTF(QQ*QQ*(YC+XC)**2+PP*PP*(XC-YS)**2)*I*5./(PP*QQ*161.)
C
C
C   *****
C
C   LIST ALL POWER SPECTRA ETC
PRINT 286,( NHT(I),I=1,27)
286  FORMAT(1H1,3X,27A4,/)
PRINT 949,(PNH(I),I=1,405)
949  FORMAT(1X,135R1,/,1X,135R1,/,1X,135R1,/)
GO TO (252,254) SSWTCHF(3)
254  PRINT 287
287  FORMAT(10X,66HFREQUENCY      COSINE AUTOCORR      SINE AUTOCORR
  1  SUM AUTOCORR//)
PRINT 289,(I,X(I),Y(I),U(I),I=1,100)
289  FORMAT(10X,I4,3F20,7)
PRINT 291

```

```

2 IMIS,MH,MM,MS,DECL
270 FORMAT(21A4,19HBASELINE PARAMETERS,37X,6HLENGTH,F10,2,6H FEET,34X
1,F16.2,12H WAVELENGTH,28X,9HELEVATION,F9,4,8H DEGREES,30X,
27HAZIMUTH,F11,4,8H DEGREES,86X,5HDELAY,F18.3,5H MICS,28X,
310HINST PHASE,F13.3,4H DEG,29X,9HFREQUENCY,F14.4,5H MC/S,28X,
410HTIME START,3I4, 34X,10HAZ START,F13.3,33X,10HEL START.
5F13.3,33X,10HPH START,F13.3,33X,10HTIME STOP,3I4, 34X,
610HAZ STOP,F13.3,33X,10HEL STOP,F13.3,33X,10HPH STOP,
7F13.3,33X,10HFRINGES ,F13,3,33X,10HINT TIME ,I10 ,8H CYCLES,
856X,5HDATE ,5X,3I4,34X,9HBANDWIDTH,F10.2,5H MC/S,32X,6HMISSES, 10,
940X,10HLOCAL H.A.,3I4,34X,3HDEC,F12,4,4H DEG)
C FLOT COSINE TRANSFORM
GO TO(910,251) SSWTCHF(3)
251 GO TO (901,262) SSWTCHF(1)
901 IF(INUM=1)233,262,237
262 WRITE (59, 230)
230 FORMAT(29H SET FOURIER TRANSFORM LIMITS)
FEAD(58,102)PA
CALL NUMBERS(PA,80,ANS,NA)
IF(NA)232,233,232
232 XTMAX=ANS(NA-1)
XTMIN=ANS(NA)
291 FORMAT(1H1,106H FREQUENCY COS TRANSFORM SIN TRANSFORM RAW P
1HASE FRINGE AMPLITUDE FRINGE PHASE SUM TRANSFORM//)
PRINT 290,(I,XT(I),YT(I),PHA(I),AMP(I),PHASE(I),TRANS(I),I=1,200)
290 FORMAT( 5X,I4,6F16.4)
GO TO 292
252 PRINT 293
293 FORMAT(20X, 93HNUMBER FRINGE AMP PHASE NUMBER FRINGE AM
1P PHASE NUMBER FRINGE AMP PHASE/)
DO 294 I=1,53
J=I+20
K=I+73
L=I+127
PRINT 253,J,AMP(J),PHASE(J),K,AMP(K),PHASE(K),L,AMP(L),PHASE(L)
253 FORMAT(14X,I12,F11.4,F10.1,I12,F11.4,F10.1,I12,F11.4,F10.1)
294 CONTINUE
C OUTPUT TAPE WILL SPACE TO END OF FILE MARK OUTPUT
292 CALL SEFF(20)
BACKSPACE 20
WRITE (20) U,X,Y,XT,YT,TRANS,PHA,PHASE,AMP,KI,T1,T2,A2,A1,E2,E1,
1 FR,IT,PCAL,AZB,ELB,DBAS,FREQ,W,F,T,ASUM,SC,PAR,NH,BW,PIINST,
2 TITLE,P1,P2,RASC,DECL
END FILE 20
BACKSPACE 20
PRINT 984
984 FORMAT(////)
PRINT 211,AZIM,ELEV,PCAL,PAMP
211 FORMAT(10X,12HMEAN AZIMUTH,F10.4,//10X,14HMEAN ELEVATION,F8.4//,
1 10X,12HFRINGE PHASE,F10.4//,10X,16HFRINGE AMPLITUDE,F12.4)
C
C *****
C
C ENCODE VARIABLES WHICH APPEAR ON GRAPHS
ENCODE(24,268,LABELX)
268 FORMAT(10X,14HCHANNEL NUMBER)
PW=ABSF(BW)
ENCODE(1456,270,INFO)TITLE,DBAS,W,ELB,AZB,DELAY,PIINST,FREQ,IH1,
1IM1,IS1,A1,E1,P1,IH2,IM2,IS2,A2,E2,P2,FR,IT,KI(2),KI(3),KI(1),EW,

```

```

265 CALL LIMITS(1.,101.,-180.,180.)
    DO 245 I=2,200,2
      XX=I/2
      YY=PHASE(I)
245 CALL POINTS(XX,YY,1R*,1)
    CALL GRIDS(1.,10.,180.,-60.)
    ENCODE(16,285,LABELY)
285 FORMAT(4X,12HFRINGE PHASE)
    CALL LABELS(LABELX,6,LABELY,4)
    CALL GRAPHS(INFO,15,364,1)
    IF(IREP)906,267,906
267 IF(OT .EQ. 1H )299,272
272 WRITE (59, 273)

233 CALL LIMITS(1.,101.,XTMIN,XTMAX)
    DO 242 I=2,200,2
      XX=I/2
      YY=XT(I)
242 CALL POINTS(XX,YY,1R*,1)
    CALL GRIDS(1.,10.,XTMAX,-(XTMAX-XTMIN)/4.)
    ENCODE(16,269,LABELY)
269 FORMAT(16HCOSINE TRANSFORM)
    CALL LABELS(LABELX,6,LABELY,4)
    CALL GRAPHS(INFO,15,364,1)
C   FLOT SINE TRANSFORM
    CALL LIMITS(1.,101.,XTMIN,XTMAX)
    DO 243 I=2,200,2
      XX=I/2
      YY=YT(I)
243 CALL POINTS(XX,YY,1R*,1)
    CALL GRIDS(1.,10.,XTMAX,-(XTMAX-XTMIN)/4.)
    ENCODE(14,280,LABELY)
280 FORMAT(14HSINE TRANSFORM)
    CALL LABELS(LABELX,6,LABELY,4)
    CALL GRAPHS(INFO,15,364,1)
    IF(IREP)906,910,906
C   FLOT FRINGE AMPLITUDE
910 GO TO (902,264) SSWTCHF(1)
902 IF(INUM=1)237,264,237
264 WRITE (59, 235)
235 FORMAT(28H SET FRINGE AMPLITUDE LIMITS)
    READ(58,102)PA
    CALL NUMBERS(PA,80,ANS,NA)
    IF(NA)236,237,236
236 AMAX=ANS(NA-1)
    AMIN=ANS(NA)
237 CALL LIMITS(1.,101.,AMIN,AMAX)
    DO 244 I=2,200,2
      XX=I/2
      YY=AMP(I)
244 CALL POINTS(XX,YY,1R*,1)
    CALL GRIDS(1.,10.,AMAX,-(AMAX-AMIN)/4.)
    ENCODE(16,282,LABELY)
282 FORMAT(16HFRINGE AMPLITUDE)
    CALL LABELS(LABELX,6,LABELY,4)
    CALL GRAPHS(INFO,15,364,1)
    IF(IREP)299,265,299
C   FLOT FRINGE PHASE

```

SIN

AMP

```

273 FORMAT(25H SET POWER SPECTRA LIMITS)
    READ(58,102)PA
    CALL NUMBERS(PA,80,ANS,NA)
    IF(NA)274,275,274
274 TMAX=ANS(NA-1)
    TMIN=ANS(NA)
275 CALL LIMITS(1.,101.,TMIN,TMAX)
    DO 276 I=2,200,2
    XX=I/2
    YY=TRANS(I)
276 CALL POINTS(XX,YY,1R*,1)
    CALL GRIDS(1.,10.,TMIN,-(TMAX-TMIN)/4,)
    FNCODE(13,277,LABELY)
277 FORMAT(13HPOWER SPECTRA)
    CALL LABELS(LABELX,6,LABELY,4)
    CALL GRAPHS(INFO,15,364,1)
299 GO TO (905,906) SSWTCHF(1)
905 ISRCH=2
    GO TO 99
C   IREP=0,NO REPLOT,1 COS AND SIN TRANS, 2 COS AND SIN TRANS,
C   3 FRINGE AMPLITUDE 4 SUM TRANSFORM
906 WRITE (59, 295)
295 FORMAT(12H REPLOT 1=4 )
    READ(58,296) IREP
296 FORMAT(I1)
    IREP=IREP+1
    GO TO(261,262,262,264,267) IREP
261 CONTINUE
    WRITE (59, 969)
969 FORMAT( 41H JUMP SWITCH 1 ON FOR NON STOP PROCESSING)
    PAUSE
    GO TO (905,970) SSWTCHF(1)
970 WRITE (59, 278)
278 FORMAT(63HTYPE 1 SKIP, 2 PROCESS, 3 REINT AND SKIP, 4 REINT AND
1PROCESS)
    READ(58,297) ISRCH
297 FORMAT(I1)
    GO TO 99
    END

```

3200 FORTRAN DIAGNOSTIC RESULTS - FOR MILSTAK

ERRORS

### Acknowledgment

The author is grateful to a large number of people who contributed to this work. J. M. Moran, Patricia P. Crowther, and J. A. Ball wrote the computer programs. G. M. Hyde, V. C. Pineo, and J. C. Carter provided engineering assistance. R. H. Erickson, R. Lewis, and D. C. Papa constructed much of the equipment. The author is particularly indebted to Professor Bernard F. Burke who initiated the project and provided much of the theoretical and practical knowledge. Finally, the author is indebted to Professor Alan H. Barrett for supervising this work as a portion of thesis research that is being undertaken at the Massachusetts Institute of Technology.



## References

1. S. Weinreb, "A Digital Spectral Analysis Technique and Its Application to Radio Astronomy," Technical Report 412, Research Laboratory of Electronics, Massachusetts Institute of Technology, Cambridge, Mass., August 30, 1963.
2. J. H. Van Vleck, Report No. 51, Radio Research Laboratory, Harvard University, Cambridge, Mass., July 21, 1943.
3. F. E. Heart, A. A. Mathiasen, and P. D. Smith, "The Haystack Computer Control System," Technical Report 406, Lincoln Laboratory, Massachusetts Institute of Technology, Lexington, Mass., 27 October 1965.
4. G. H. Conant, "Radiometric Spectral-Line Processing in the Haystack Antenna Pointing System" (in preparation for publication).

-  
-  
-

-  
-  
-



JOINT SERVICES ELECTRONICS PROGRAM  
REPORTS DISTRIBUTION LIST

Department of Defense

Dr. Edward M. Reilley  
Asst Director (Research)  
Ofc of Defense Res & Eng  
Department of Defense  
Washington, D.C. 20301

Office of Deputy Director  
(Research and Information Room 3D1037)  
Department of Defense  
The Pentagon  
Washington, D.C. 20301

Director  
Advanced Research Projects Agency  
Department of Defense  
Washington, D.C. 20301

Director for Materials Sciences  
Advanced Research Projects Agency  
Department of Defense  
Washington, D.C. 20301

Headquarters  
Defense Communications Agency (333)  
The Pentagon  
Washington, D.C. 20305

Defense Documentation Center  
Attn: TISIA  
Cameron Station, Bldg. 5  
Alexandria, Virginia 22314

Director  
National Security Agency  
Attn: Librarian C-332  
Fort George G. Meade, Maryland 20755

Weapons Systems Evaluation Group  
Attn: Col. Daniel W. McElwee  
Department of Defense  
Washington, D.C. 20305

National Security Agency  
Attn: R4-James Tippet  
Office of Research  
Fort George G. Meade, Maryland 20755

Central Intelligence Agency  
Attn: OCR/DD Publications  
Washington, D.C. 20505

Department of the Air Force

Colonel Kee  
AFRSTE  
Hqs. USAF  
Room ID-429, The Pentagon  
Washington, D.C. 20330

Colonel A. Swan  
Aerospace Medical Division  
Brooks Air Force Base, Texas 78235

AUL3T-9663  
Maxwell AFB, Alabama 36112

AFFTC (FTBPP-2)  
Technical Library  
Edwards AFB, Calif. 93523

Space Systems Division  
Air Force Systems Command  
Los Angeles Air Force Station  
Los Angeles, California 90045  
Attn: SSSD

Major Charles Waespy  
Technical Division  
Deputy for Technology  
Space Systems Division, AFSC  
Los Angeles, California 90045

SSD(SSSTR/Lt. Starbuck)  
AFUPO  
Los Angeles, California 90045

Det #6, OAR (LOOAR)  
Air Force Unit Post Office  
Los Angeles, California 90045

Systems Engineering Group (RTD)  
Technical Information Reference Branch  
Attn: SEPIR  
Directorate of Engineering Standards  
and Technical Information  
Wright-Patterson AFB, Ohio 45433

ARL (ARIY)  
Wright-Patterson AFB, Ohio 45433

Dr. H. V. Noble  
Air Force Avionics Laboratory  
Wright-Patterson AFB, Ohio 45433

Mr. Peter Murray  
Air Force Avionics Laboratory  
Wright-Patterson AFB, Ohio 45433

JOINT SERVICES REPORTS DISTRIBUTION LIST (continued)

AFAL (AVTE/R. D. Larson)  
Wright-Patterson AFB, Ohio 45433

Commanding General  
Attn: STEWS-WS-VT  
White Sands Missile Range  
New Mexico 88002

RADC (EMLAL-1)  
Griffiss AFB, New York 13442  
Attn: Documents Library

Academy Library (DFSLB)  
U.S. Air Force Academy  
Colorado Springs, Colorado 80912

Lt. Col. Bernard S. Morgan  
Frank J. Seiler Research Laboratory  
U.S. Air Force Academy  
Colorado Springs, Colorado 80912

APGC (PGBPS-12)  
Eglin AFB, Florida 32542

AFETR Technical Library  
(ETV, MU-135)  
Patrick AFB, Florida 32925

AFETR (ETLLG-1)  
STINFO Officer (for Library)  
Patrick AFB, Florida 32925

Dr. L. M. Hollingsworth  
AFCL (CRN)  
L. G. Hanscom Field  
Bedford, Massachusetts 01731

AFCL (CRMCLR)  
AFCL Research Library, Stop 29  
L. G. Hanscom Field  
Bedford, Massachusetts 01731

Colonel Robert E. Fontana  
Department of Electrical Engineering  
Air Force Institute of Technology  
Wright-Patterson AFB, Ohio 45433

Colonel A. D. Blue  
RTD (RTTL)  
Bolling Air Force Base, D.C. 20332

Dr. I. R. Mirman  
AFSC (SCT)  
Andrews Air Force Base, Maryland 20331

Colonel J. D. Warthman  
AFSC (SCTR)  
Andrews Air Force Base, Maryland 20331

Lt. Col. J. L. Reeves  
AFSC (SCBB)  
Andrews Air Force Base, Maryland 20331

ESD (ESTI)  
L. G. Hanscom Field  
Bedford, Massachusetts 01731

AEDC (ARO, INC)  
Attn: Library/Documents  
Arnold AFS, Tennessee 37389

European Office of Aerospace Research  
Shell Building  
47 Rue Cantersteen  
Brussels, Belgium

Lt. Col. Robert B. Kalisch  
Chief, Electronics Division  
Directorate of Engineering Sciences  
Air Force Office of Scientific Research  
Arlington, Virginia 22209

Department of the Army

U.S. Army Research Office  
Attn: Physical Sciences Division  
3045 Columbia Pike  
Arlington, Virginia 22204

Research Plans Office  
U.S. Army Research Office  
3045 Columbia Pike  
Arlington, Virginia 22204

Commanding General  
U.S. Army Materiel Command  
Attn: AMCRD-RS-DE-E  
Washington, D.C. 20315

Commanding General  
U.S. Army Strategic Communications  
Command  
Washington, D.C. 20315

Commanding Officer  
U.S. Army Materials Research Agency  
Watertown Arsenal  
Watertown, Massachusetts 02172

Commanding Officer  
U.S. Army Ballistics Research Laboratory  
Attn: V. W. Richards  
Aberdeen Proving Ground  
Aberdeen, Maryland 21005

JOINT SERVICES REPORTS DISTRIBUTION LIST (continued)

<p>Commandant U.S. Army Air Defense School Attn: Missile Sciences Division C&amp;S Dept. P. O. Box 9390 Fort Bliss, Texas 79916</p>	<p>Commanding Officer U.S. Army Research Office (Durham) Attn: CRD-AA-IP (Richard O. Ulsh) Box CM, Duke Station Durham, North Carolina 27706</p>																												
<p>Commanding General U.S. Army Missile Command Attn: Technical Library Redstone Arsenal, Alabama 35809</p>	<p>Librarian U.S. Army Military Academy West Point, New York 10996</p>																												
<p>Commanding General Frankford Arsenal Attn: L600-64-4 (Dr. Sidney Ross) Philadelphia, Pennsylvania 19137</p>	<p>The Walter Reed Institute of Research Walter Reed Medical Center Washington, D.C. 20012</p>																												
<p>U.S. Army Munitions Command Attn: Technical Information Branch Picatinny Arsenal Dover, New Jersey 07801</p>	<p>Commanding Officer U.S. Army Engineer R&amp;D Laboratory Attn: STINFO Branch Fort Belvoir, Virginia 22060</p>																												
<p>Commanding Officer Harry Diamond Laboratories Attn: Dr. Berthold Altman (AMXDO-TI) Connecticut Avenue and Van Ness St. N. W. Washington, D.C. 20438</p>	<p>Commanding Officer U.S. Army Electronics R&amp;D Activity White Sands Missile Range, New Mexico 88002</p>																												
<p>Commanding Officer U.S. Army Security Agency Arlington Hall Arlington, Virginia 22212</p>	<p>Dr. S. Benedict Levin, Director Institute for Exploratory Research U.S. Army Electronics Command Fort Monmouth, New Jersey 07703</p>																												
<p>Commanding Officer U.S. Army Limited War Laboratory Attn: Technical Director Aberdeen Proving Ground Aberdeen, Maryland 21005</p>	<p>Director Institute for Exploratory Research U.S. Army Electronics Command Attn: Mr. Robert O. Parker, Executive Secretary, JSTAC (AMSEL-XL-D) Fort Monmouth, New Jersey 07703</p>																												
<p>Commanding Officer Human Engineering Laboratories Aberdeen Proving Ground, Maryland 21005</p>	<p>Commanding General U.S. Army Electronics Command Fort Monmouth, New Jersey 07703 Attn: AMSEL-SC</p>																												
<p>Director U.S. Army Engineer Geodesy, Intelligence and Mapping Research and Development Agency Fort Belvoir, Virginia 22060</p>	<table border="0"> <tbody> <tr> <td>RD-D</td> <td>NL-D</td> </tr> <tr> <td>RD-G</td> <td>NL-A</td> </tr> <tr> <td>RD-GF</td> <td>NL-P</td> </tr> <tr> <td>RD-MAT</td> <td>NL-R</td> </tr> <tr> <td>XL-D</td> <td>NL-S</td> </tr> <tr> <td>XL-E</td> <td>KL-D</td> </tr> <tr> <td>XL-C</td> <td>KL-E</td> </tr> <tr> <td>XL-S</td> <td>KL-S</td> </tr> <tr> <td>HL-D</td> <td>KL-TM</td> </tr> <tr> <td>HL-CT-R</td> <td>KL-TQ</td> </tr> <tr> <td>HL-CT-P</td> <td>KL-TS</td> </tr> <tr> <td>HL-CT-L</td> <td>VL-D</td> </tr> <tr> <td>HL-CT-O</td> <td>WL-D</td> </tr> <tr> <td>HL-CT-I</td> <td></td> </tr> </tbody> </table>	RD-D	NL-D	RD-G	NL-A	RD-GF	NL-P	RD-MAT	NL-R	XL-D	NL-S	XL-E	KL-D	XL-C	KL-E	XL-S	KL-S	HL-D	KL-TM	HL-CT-R	KL-TQ	HL-CT-P	KL-TS	HL-CT-L	VL-D	HL-CT-O	WL-D	HL-CT-I	
RD-D	NL-D																												
RD-G	NL-A																												
RD-GF	NL-P																												
RD-MAT	NL-R																												
XL-D	NL-S																												
XL-E	KL-D																												
XL-C	KL-E																												
XL-S	KL-S																												
HL-D	KL-TM																												
HL-CT-R	KL-TQ																												
HL-CT-P	KL-TS																												
HL-CT-L	VL-D																												
HL-CT-O	WL-D																												
HL-CT-I																													
<p>Commandant U.S. Army Command and General Staff College Attn: Secretary Fort Leavenworth, Kansas 66270</p>																													
<p>Dr. H. Robl, Deputy Chief Scientist U.S. Army Research Office (Durham) Box CM, Duke Station Durham, North Carolina 27706</p>																													

JOINT SERVICES REPORTS DISTRIBUTION LIST (continued)

Department of the Navy

Chief of Naval Research  
Department of the Navy  
Washington, D.C. 20360  
Attn: Code 427

Naval Electronics Systems Command  
ELEX 03  
Falls Church, Virginia 22046

Naval Ship Systems Command  
SHIP 031  
Washington, D.C. 20360

Naval Ship Systems Command  
SHIP 035  
Washington, D.C. 20360

Naval Ordnance Systems Command  
ORD 32  
Washington, D.C. 20360

Naval Air Systems Command  
AIR 03  
Washington, D.C. 20360

Commanding Officer  
Office of Naval Research Branch Office  
Box 39, Navy No 100 F. P. O.  
New York, New York 09510

Commanding Officer  
Office of Naval Research Branch Office  
219 South Dearborn Street  
Chicago, Illinois 60604

Commanding Officer  
Office of Naval Research Branch Office  
1030 East Green Street  
Pasadena, California 91101

Commanding Officer  
Office of Naval Research Branch Office  
207 West 24th Street  
New York, New York 10011

Commanding Officer  
Office of Naval Research Branch Office  
495 Summer Street  
Boston, Massachusetts 02210

Director, Naval Research Laboratory  
Technical Information Officer  
Washington, D.C. 20360  
Attn: Code 2000

Commander  
Naval Air Development and Material Center  
Johnsville, Pennsylvania 18974

Librarian  
U.S. Naval Electronics Laboratory  
San Diego, California 95152

Commanding Officer and Director  
U.S. Naval Underwater Sound Laboratory  
Fort Trumbull  
New London, Connecticut 06840

Librarian  
U.S. Navy Post Graduate School  
Monterey, California 93940

Commander  
U.S. Naval Air Missile Test Center  
Point Magu, California 93041

Director  
U.S. Naval Observatory  
Washington, D.C. 20390

Chief of Naval Operations  
OP-07  
Washington, D.C. 20350

Director, U.S. Naval Security Group  
Attn: G43  
3801 Nebraska Avenue  
Washington, D.C. 20390

Commanding Officer  
Naval Ordnance Laboratory  
White Oak, Maryland 21502

Commanding Officer  
Naval Ordnance Laboratory  
Corona, California 91720

Commanding Officer  
Naval Ordnance Test Station  
China Lake, California 93555

Commanding Officer  
Naval Avionics Facility  
Indianapolis, Indiana 46241

Commanding Officer  
Naval Training Device Center  
Orlando, Florida 32811

U.S. Naval Weapons Laboratory  
Dahlgren, Virginia 22448

JOINT SERVICES REPORTS DISTRIBUTION LIST (continued)

Weapons Systems Test Division  
Naval Air Test Center  
Patuxent River, Maryland 20670  
Attn: Library

Head, Technical Division  
U.S. Naval Counter Intelligence  
Support Center  
Fairmont Building  
4420 North Fairfax Drive  
Arlington, Virginia 22203

NASA Scientific & Technical Information  
Facility  
Attn: Acquisitions Branch (S/AK/DL)  
P. O. Box 33,  
College Park, Maryland 20740

NASA, Langley Research Center  
Langley Station  
Hampton, Virginia 23365  
Attn: Mr. R. V. Hess, Mail Stop 160

Other Government Agencies

Mr. Charles F. Yost  
Special Assistant to the Director  
of Research  
National Aeronautics and  
Space Administration  
Washington, D.C. 20546

Dr. H. Harrison, Code RRE  
Chief, Electrophysics Branch  
National Aeronautics and  
Space Administration  
Washington, D.C. 20546

Goddard Space Flight Center  
National Aeronautics and  
Space Administration  
Attn: Library C3/TDL  
Green Belt, Maryland 20771

NASA Lewis Research Center  
Attn: Library  
21000 Brookpark Road  
Cleveland, Ohio 44135

National Science Foundation  
Attn: Dr. John R. Lehmann  
Division of Engineering  
1800 G Street, N. W.  
Washington, D.C. 20550

U.S. Atomic Energy Commission  
Division of Technical Information Extension  
P. O. Box 62  
Oak Ridge, Tennessee 37831

Los Alamos Scientific Laboratory  
Attn: Reports Library  
P. O. Box 1663  
Los Alamos, New Mexico 87544

Non-Government Agencies

Director  
Research Laboratory of Electronics  
Massachusetts Institute of Technology  
Cambridge, Massachusetts 02139

Polytechnic Institute of Brooklyn  
55 Johnson Street  
Brooklyn, New York 11201  
Attn: Mr. Jerome Fox  
Research Coordinator

Director  
Columbia Radiation Laboratory  
Columbia University  
538 West 120th Street  
New York, New York 10027

Director  
Coordinated Science Laboratory  
University of Illinois  
Urbana, Illinois 61803

Director  
Stanford Electronics Laboratories  
Stanford University  
Stanford, California 94305

Director  
Electronics Research Laboratory  
University of California  
Berkeley, California 94720

Director  
Electronic Sciences Laboratory  
University of Southern California  
Los Angeles, California 90007

Professor A. A. Dougal, Director  
Laboratories for Electronics and  
Related Sciences Research  
University of Texas  
Austin, Texas 78712

JOINT SERVICES REPORTS DISTRIBUTION LIST (continued)

Gordon McKay Library A175  
Technical Reports Collection  
Harvard College  
Cambridge, Massachusetts 02138

Aerospace Corporation  
P.O. Box 95085  
Los Angeles, California 90045  
Attn: Library Acquisitions Group

Professor Nicholas George  
California Institute of Technology  
Pasadena, California 91109

Aeronautics Library  
Graduate Aeronautical Laboratories  
California Institute of Technology  
1201 E. California Blvd.  
Pasadena, California 91109

Director, USAF Project RAND  
Via: Air Force Liaison Office  
The RAND Corporation  
1700 Main Street  
Santa Monica, California 90406  
Attn: Library

The Johns Hopkins University  
Applied Physics Laboratory  
8621 Georgia Avenue  
Silver Spring, Maryland 20910  
Attn: Boris W. Kuvshinoff  
Document Librarian

Hunt Library  
Carnegie Institute of Technology  
Schenley Park  
Pittsburgh, Pennsylvania 15213

Dr. Leo Young  
Stanford Research Institute  
Menlo Park, California 94025

Mr. Henry L. Bachmann  
Assistant Chief Engineer  
Wheeler Laboratories  
122 Cuttermill Road  
Great Neck, New York 11021

School of Engineering Sciences  
Arizona State University  
Tempe, Arizona 85281

Engineering and Mathematical  
Sciences Library  
University of California  
405 Hilgrad Avenue  
Los Angeles, California 90024

California Institute of Technology  
Pasadena, California 91109  
Attn: Documents Library

University of California  
Santa Barbara, California 93106  
Attn: Library

Carnegie Institute of Technology  
Electrical Engineering Department  
Pittsburgh, Pennsylvania 15213

University of Michigan  
Electrical Engineering Department  
Ann Arbor, Michigan 48104

New York University  
College of Engineering  
New York, New York 10019

Syracuse University  
Dept. of Electrical Engineering  
Syracuse, New York 13210

Yale University  
Engineering Department  
New Haven, Connecticut 06520

Airborne Instruments Laboratory  
Deerpark, New York 11729

Bendix Pacific Division  
11600 Sherman Way  
North Hollywood, California 91605

General Electric Company  
Research Laboratories  
Schenectady, New York 12301

Lockheed Aircraft Corporation  
P.O. Box 504  
Sunnyvale, California 94088

Raytheon Company  
Bedford, Massachusetts 01730  
Attn: Librarian

Dr. G. J. Murphy  
The Technological Institute  
Northwestern University  
Evanston, Illinois 60201

Dr. John C. Hancock, Director  
Electronic Systems Research Laboratory  
Purdue University  
Lafayette, Indiana 47907



JOINT SERVICES REPORTS DISTRIBUTION LIST (continued)

Director  
Microwave Laboratory  
Stanford University  
Stanford, California 94305

Emil Schafer Head  
Electronics Properties Info Center  
Hughes Aircraft Company  
Culver City, California 90230

1  
2  
3

4  
5  
6



UNCLASSIFIED

Security Classification

3ND PPSO 13152

DOCUMENT CONTROL DATA - R&D		
<i>(Security classification of title, body of abstract and indexing annotation must be entered when the overall report is classified)</i>		
1. ORIGINATING ACTIVITY <i>(Corporate author)</i> Research Laboratory of Electronics Massachusetts Institute of Technology Cambridge, Massachusetts		2 a. REPORT SECURITY CLASSIFICATION Unclassified
		2 b. GROUP None
3. REPORT TITLE The Haystack-Millstone Interferometer System		
4. DESCRIPTIVE NOTES <i>(Type of report and inclusive dates)</i> Technical Report		
5. AUTHOR(S) <i>(Last name, first name, initial)</i> Rogers, Alan E. E.		
6. REPORT DATE March 15, 1967	7 a. TOTAL NO. OF PAGES 60	7 b. NO. OF REFS 4
8 a. CONTRACT OR GRANT NO. DA 28-043-AMC-02536(E)	9 a. ORIGINATOR'S REPORT NUMBER(S) Technical Report 457	
b. PROJECT NO. 200-14501-B31F NASA Grant NsG-419	9 b. OTHER REPORT NO(S) <i>(Any other numbers that may be assigned this report)</i>	
10. AVAILABILITY/LIMITATION NOTICES Distribution of this report is unlimited.		
11. SUPPLEMENTARY NOTES	12. SPONSORING MILITARY ACTIVITY Joint Services Electronics Program thru USAECOM, Fort Monmouth, N. J.	
13. ABSTRACT  The Haystack 120-ft antenna and the Millstone 84-ft antenna have been coupled together to form a radiometric interferometer. At 18-cm wavelength, which was chosen for a study of galactic OH emission, the interferometer has a minimum fringe spacing of 54 seconds of arc. The interferometer synthesizes a beam approximately equivalent to that of a 2000-ft parabolic antenna and can measure positions to a small fraction of the fringe spacing. The interferometer uses a digital correlator to analyze the fringe amplitude and phase as a function of frequency. This enables mapping of spectral features. The design and construction are described, as well as the theory and method of data reduction. A noise analysis shows that the threshold level could be reduced by using more complex processing techniques. It is shown that for radiometric studies many of the capabilities of a very large antenna can be synthesized, with smaller antennas and complex data-processing equipment taking the place of mechanical structure.		

DD FORM 1473

1 JAN 64

11A 0101 807 6800

UNCLASSIFIED

Security Classification

**UNCLASSIFIED**

Security Classification

14. KEY WORDS	LINK A		LINK B		LINK C	
	ROLE	WT	ROLE	WT	ROLE	WT
Radiometric interferometer Haystack Millstone Noise analysis Digital correlator Spectral line interferometer aperture synthesis Radio Astronomy Servo-controlled transmission line Microwave interferometer						

**DD FORM 1473** (BACK)  
1 NOV 55

S/N 0101-807-6821

**UNCLASSIFIED**

Security Classification

A-31409